First-forbidden β decay in the lead region and mesonic enhancement of the weak axial current

E. K. Warburton
Brookhaven National Laboratory, Upton, New York 11973
(Received 17 January 1991)

A shell-model study is made of first-forbidden β decay and related processes in $A = 205$–212 nuclei. The interactions used are modifications of the Kuo-Herling realistic effective interactions for particles above and holes below ^{208}Pb and a cross-shell G-matrix interaction connecting these two. Large-scale diagonalizations are made of 1p-1h excitations across the double-shell closure at ^{208}Pb. The calculations of the first-forbidden rates use effective single-particle matrix elements which incorporate core polarization of the final state to first order. All first-order initial state 1p-1h admixtures are included explicitly in the diagonalization. A least-squares fit of theory to experiment for eighteen $\Delta J = 0$ and 1 decay rates was made with two unknowns: (1) an enhancement factor $\epsilon_{\rm mec}$ for the rank-zero matrix element of γ_5, and (2) an overall scaling factor for the rank-one component of the decay rate. A good fit is achieved yielding $\epsilon_{\rm mec} = 2.01 \pm 0.05$ and a rank-one scaling factor of 0.97 ± 0.06. The agreement of the latter with unity indicates a satisfactory understanding of the rank-one component of the decay. The result $\epsilon_{\rm mec} = 2.01 \pm 0.05$ indicates an enhancement of the matrix element of γ_5 by 100% over the impulse approximation. A 40% effect is predicted from meson exchange. Thus, a deficiency in the meson-exchange calculation or some further as-yet-unforseen contribution is suggested. Predictions for twenty other decays in $A = 205$–211 nuclei are compared to experiment and found to be in good general agreement. A calculation of the capture of neutrinos by ^{205}Tl is described in detail.

I. INTRODUCTION

In 1978 Kubodera, Delorme, and Rho [1] and Guichon, *et al.* [2] predicted a large meson-exchange-current (mec) contribution to the timelike component of the weak axial current γ_5 in the nuclear medium. The enhancement over the impulse approximation is predicted to be ~ 40–$70\,\%$ and to be insensitive to nuclear structure [3–8]. The prediction is based on chiral-symmetry arguments and soft-pion theorems and is insensitive to the details of the meson exchange. This is in contrast to other mesonic effects such as occur for $M1$ and Gamow-Teller processes and which involve complicated dependencies on π and ρ mesons, isobar currents, etc. [9]. The mec enhancement of the timelike component of the weak axial current, i.e., the matrix element of γ_5, is most easily observed via its effect on first-forbidden beta-decay rates since γ_5 is one of the two operators contributing to the rank-zero component of first-forbidden decays. The prediction of this very large mec enhancement stimulated a great deal of experimental and theoretical activity. Most of the activity centered on the $A = 16$ region and theoretical studies are still being carried out there [10]. Results for $A \sim 16$ have been reviewed by Towner [8], Warburton [11], and Millener and Warburton [12]. The available data for $A \sim 40$ was examined for possible evidence of mec effects [13] and some evidence was found. One case at $A = 96$, namely $^{96}\mathrm{Y}(0^-) \rightarrow {}^{96}\mathrm{Zr}(0^+)$, was shown to suggest an enhancement of $\sim 70\%$ [14].

Until this present work there had been no detailed study of mec effects in first-forbidden decays in the lead region. This is startling for two reasons. First, because, as illustrated in Fig. 1 and Table I, the lead region provides a large number of first-forbidden decays among which are the fastest known. Second, because there was a great deal of theoretical interest in first-forbidden decays in this region prior to and just after the mec predictions in 1978 [16–19]. Furthermore, this pre-1978 work left unexplained discrepancies and unresolved inconsistencies in the comparison of theoretical predictions to experiment. The fact that the activity has been centered on $A \sim 16$ with none at $A \sim 208$ is even more surprising after one becomes familiar with the systematics of both regions; there is no doubt that the shell-model calculations necessary to display the mec enhancement are more accurate at $A \sim 208$ than at $A \sim 16$ and near ^{208}Pb the effect is more transparently and accurately exposed. One reason for the decade-long neglect of the lead region by those interested in the mec effect is the small overlap between studies in the two regions. There are several instances where effects well-known to practitioners in one region are unknown to those in the other. Also, there seems to be a lack of awareness of the different behavior of the decays in the two regions. In the present work some attempt will be made to redress this insularity. The same formalism will be used for first-forbidden decays throughout the periodic table and an attempt will be made to relate results in the lead region to those in the $A \sim 16$ region.

II. THE SHELL-MODEL INTERACTIONS

The β-decay matrix elements are calculated in the usual way:

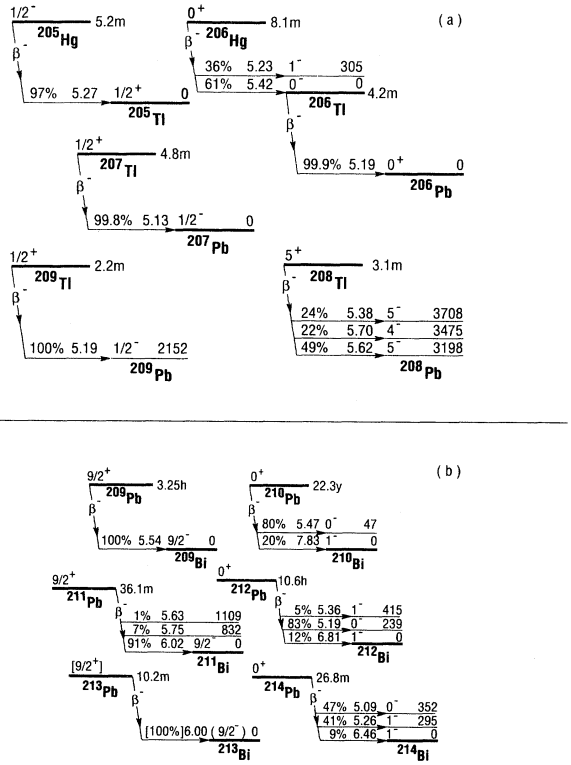

FIG. 1. (a) First-forbidden decays in $A = 205$–208 nuclei. (b) First-forbidden decays in $A = 209$–214 nuclei. The branching ratio and the $\log f_0 t$ value are given for each branch. The data are from Ref. [15].

$$M_R^\alpha = \sum_{j_i j_f} \mathcal{M}_R^\alpha(j_i j_f) = \sum_{j_i j_f} D_R(j_i j_f) M_R^\alpha(j_i j_f, \text{eff})$$
$$= \sum_{j_i j_f} D_R(j_i j_f) q_\alpha(j_i j_f) M_R^\alpha(j_i j_f). \quad (1)$$

Equation (1) introduces notation to be used throughout this article. In Eq. (1) α labels the specific matrix element of rank R, $M_R^\alpha(j_i j_f)$ is a single-particle matrix element for the transition $j_i \rightarrow j_f$ in the impulse approximation, and the quenching factor $q_\alpha(j_i j_f)$ corrects $M_R^\alpha(j_i j_f)$ for the finite size of the model space and some effects of the nuclear medium so that the *effective* value of $M_R^\alpha(j_i j_f)$ is $q_\alpha(j_i j_f) M_R^\alpha(j_i j_f) \equiv M_R^\alpha(j_i j_f, \text{eff})$. The $D_R(j_i j_f)$ are the one-body transition densities which are the result of the shell-model calculations. The calculations were carried out with the spherical shell-model code OXBASH [20]. A complete set of calculations for all $A = 205$–212 nuclei of Fig. 1 was performed with both a surface-delta interaction (SDI) and a combination of realistic interactions based on G-matrix descriptions of nucleon-nucleon potentials.

A. The Poppelier-Glaudemans interaction

The SDI interaction used is that of Poppelier and Glaudemans [21] which has a model space consisting of the four closest orbits below and the three above the $Z = 82$, $N = 126$ energy gap for both protons and neutrons (see Fig. 2). The single-particle energies and the two other parameters of the SDI were determined by a

TABLE I. Fast $\Delta J = 0, 1$ first-forbidden β^- transitions in the lead region. For the last five columns the number in parenthesis is the uncertainty in the least significant figure. For f_0, the number in square brackets is the power of ten. The data are from Ref. [15].

Transition		E_x	$T_{\frac{1}{2}}$	Q_β	f_0	BR	$\log f_0 t$
Initial	Final	(keV)		(keV)		(%)	
^{205}Hg($\frac{1}{2}^-$)	^{205}Tl($\frac{1}{2}^+$)	0	312(6) s	1534(5)	5.84(7)[+2]	96.8(15)	5.274(12)
^{206}Hg(0^+)	^{206}Tl(0^-)	0	489(6) s	1309(20)	3.25(18)[+2]	61.0(120)	5.42(9)
^{206}Hg(0^+)	^{206}Tl(1^-)	305	489(6) s	1004(20)	1.25(9)[+2]	36.0(70)	5.23(9)
^{206}Tl(0^-)	^{206}Pb(0^+)	0	252(1) s	1531(4)	6.08(6)[+2]	99.91(2)	5.184(5)
^{207}Tl($\frac{1}{2}^+$)	^{207}Pb($\frac{1}{2}^-$)	0	286(1) s	1427(6)	4.69(7)[+2]	99.76(4)	5.128(7)
^{208}Tl(5^+)	^{208}Pb(5^-)	3198	183.2(2) s	1800(4)	1.10(1)[+3]	48.7(12)	5.619(11)
^{208}Tl(4^+)	^{208}Pb(4^-)	3475	183.2(2) s	1523(4)	5.96(6)[+2]	21.8(4)	5.700(9)
^{208}Tl(5^+)	^{208}Pb(5^-)	3708	183.2(2) s	1290(4)	3.20(4)[+2]	24.5(6)	5.379(12)
^{209}Tl($\frac{1}{2}^+$)	^{209}Pb($\frac{1}{2}^-$)	2152	132(4) s	1824(12)	1.17(3)[+3]	100.0	5.189(17)
^{209}Pb($\frac{9}{2}^+$)	^{209}Bi($\frac{9}{2}^-$)	0	195.2(8) m	644(1)	2.99(2)[+1]	100.0	5.544(3)
^{210}Pb(0^+)	^{210}Bi(1^-)	0	22.3(2) y	63.1(5)	1.91(5)[−2]	20.0(30)	7.827(66)
^{210}Pb(0^+)	^{210}Bi(0^-)	47	22.3(2) y	16.6(5)	3.3(3)[−4]	80.0(30)	5.468(43)
^{211}Pb($\frac{9}{2}^+$)	^{211}Bi($\frac{9}{2}^-$)	0	36.1(2) m	1379(6)	4.34(7)[+2]	90.86(19)	6.015(7)
^{211}Pb($\frac{9}{2}^+$)	^{211}Bi($\frac{9}{2}^-$)	832	36.1(2) m	547(6)	1.72(6)[+1]	6.58(16)	5.754(19)
^{211}Pb($\frac{9}{2}^+$)	^{211}Bi($\frac{9}{2}^-$)	1109	36.1(2) m	270(6)	1.72(12)[+0]	0.88(4)	5.627(37)
^{212}Pb(0^+)	^{212}Bi(1^-)	0	10.64(1) h	571(4)	1.99(5)[+1]	11.8(24)	6.809(90)
^{212}Pb(0^+)	^{212}Bi(0^-)	239	10.64(1) h	332(4)	3.36(13)[+0]	83.2(24)	5.190(20)
^{212}Pb(0^+)	^{212}Bi(1^-)	415	10.64(1) h	156(4)	3.07(24)[−1]	5.09(17)	5.363(38)
^{214}Pb(0^+)	^{214}Bi(1^-)	0	26.8(9) m	1030(11)	1.52(6)[+2]	8.5(1)	6.459(56)
^{214}Pb(0^+)	^{214}Bi(1^-)	295	26.8(9) m	735(11)	4.68(24)[+1]	41.09(24)	5.263(27)
^{214}Pb(0^+)	^{214}Bi(0^-)	352	26.8(9) m	678(11)	3.56(20)[+1]	46.7(7)	5.088(29)

least-squares fit to 74 experimental energies in $A = 207$–209 nuclei assuming at most 1p-1h (one-particle-one-hole) excitations relative to the doubly closed $Z = 82$, $N = 126$ (^{208}Pb) core. This interaction gives quite good agreement with binding energies and other observables with some exceptions which will be discussed in Sec. IV A.

B. The Kuo-Herling hole and particle interactions

The residual interaction of Kuo and Herling [22] was derived by reaction matrix techniques [23] from a free nucleon-nucleon potential [24] with renormalizations due to the finite extension of the model space (Fig. 2). The fact that effective realistic residual interactions give a good description of nuclei near closed shells throughout the periodic table is a great success for nuclear structure. Nevertheless, shell-model calculations have revealed significant discrepancies [25–27] in the Kuo-Herling interaction which can be laid to approximations made for reasons of computational simplicity. For each two-body-matrix-element (TBME) the Kuo-Herling interaction has a bare matrix element, a 1p-1h core polarization "bubble" and a further renormalization due to 2p-2h excitations. Single particle energies (SPE) are taken from the experimental spectra of $A = 207$–209 and are shown in Fig. 2. Better agreement with experiment is obtained if the 2p-2h part of the interaction is omitted [25, 26] and this we do. A very large improvement is gained by tuning selected TBME to match experimental binding energies [28, 29, 26]. The Kuo-Herling interaction is in two unconnected parts, a hole interaction, KHH, for nuclei below ^{208}Pb and a particle interaction, KHP, for nuclei above ^{208}Pb. In a previous study [26] the best fit to experimental energy spectra was found as a function of K_{ph} for

$$\langle j_1 j_2 | V | j_3 j_4 \rangle = \langle j_1 j_2 | V | j_3 j_4 \rangle_{\text{bare}} + K_{ph} \langle j_1 j_2 | V | j_3 j_4 \rangle_{\text{1p-1h}}. \quad (2)$$

The justification for Eq. (2) and the adjustment of the 1p-1h strength is discussed in detail by Warburton and Brown [26]. The modified Kuo-Herling particle space—labeled KHP_e to distinguish it from the unmodified KHP interaction—also has some proton-neutron TBME varied so as to match the experimental spectrum of ^{210}Bi for $E_x < 2.0$ MeV [26]. The KHP_e interaction is used to describe the $A = 210$–212 decays.

We designate the Kuo-Herling hole interaction with $K_{ph} = 1$ as KHH. The "tuned" form of this interaction—designated KHH_e—uses the changes published by Rydström *et al.* [28] for the proton-proton (pp) and proton-neutron (pn) parts of the interaction and a modification starting from $K_{ph} = 0.75$ for the neutron-neutron (nn) part. This latter nn part, due to McGrory [29], also has 52 diagonal TBME varied so as to better reproduce the experimental spectrum of ^{206}Pb and ^{204}Pb. The KHH_e interaction is used to describe the $A = 205$ and 206 decays.

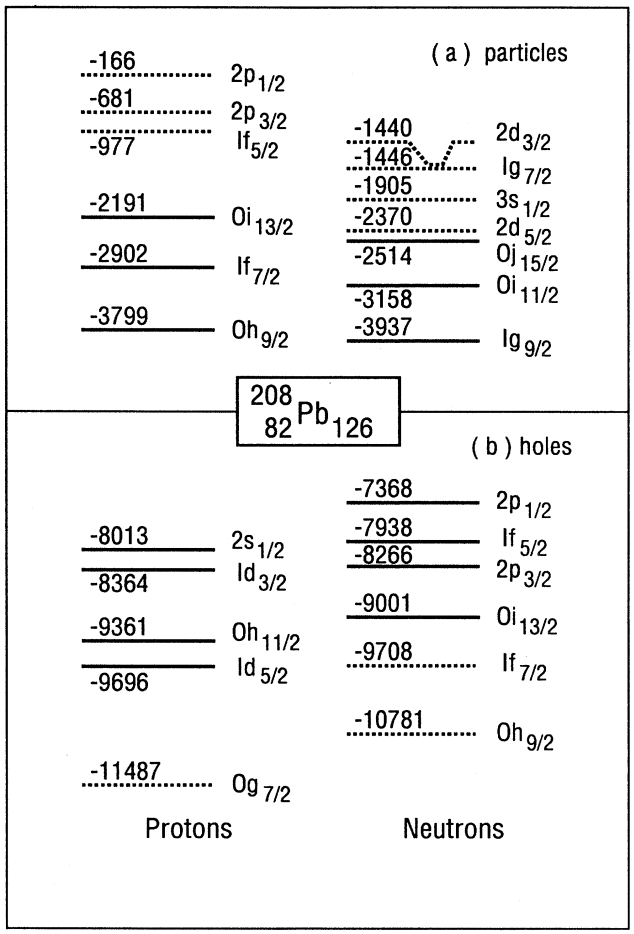

FIG. 2. The Kuo-Herling and Poppelier-Kuo-Herling (PKH) model spaces. Single-particle energies are taken from experiment and given in keV. The Kuo-Herling interaction is for either (a) particles above ^{208}Pb or (b) holes below ^{208}Pb. Each includes all the particle or hole orbits shown. The two model spaces are not connected. The PKH model space consists of the orbits denoted by solid lines. The interaction includes excitation across the $Z = 82$, $N = 126$ energy gap, i.e., the particle and hole spaces are connected. It uses the same single-particle energies as the KH interactions which are different than those of the Poppelier-Glaudemans interaction (Ref. [21]).

C. PKH: a cross-shell interaction

In order to incorporate 1p-1h excitations into the calculations performed with the KHH_e and KHP_e interactions and to calculate the $A = 207$–209 decays, an interaction which connects the KHH and KHP model spaces is desirable. Experience with the Poppelier-Glaudemans SDI interaction demonstrated the utility of its model space for the $A = 205$–212 decays of interest. Thus, an interaction (PKH) was constructed in the Poppelier-Glaudemans model space with the KHH and KHP interactions connected by 1p-1h TBME. Single-particle energies were taken from experiment and thus are the same

as for the KH interaction (Fig. 2). The model space consists of all the orbit denoted by solid lines in Fig. 2. The particle-particle and hole-hole parts of the PKH interaction were obtained by truncating the two KH interactions to this model space, i.e., omitting the orbits denoted by dotted lines. To compensate for this truncation the K_{ph} of Eq. (2) was increased so as to best reproduce the spectra of $A = 204$–206 and 210–212 nuclei in the manner previously described [26]. For the pp and pn parts of the KHH_e interaction no change was made because the low-lying states were effected very little by the truncation. For the nn part of KHH_e, a significant improvement in the spectra of ^{204,206}Pb was found if the omission of the $\nu 0h_{9/2}$ and $\nu 1f_{7/2}$ orbits was compensated for by adding $0.60\langle j_1 j_2|V|j_3 j_4\rangle_{\text{1p-1h}}$ to each TBME. For the KHP interaction, the values of K_{ph} determined for the pp and nn parts of the interaction were 1.16 and 1.56 (as opposed to 0.92 and 1.07 for the untruncated KHP_e model space [26]). The pn part of the interaction was left unchanged since the low-lying states of ^{210}Bi were not significantly affected by the truncation.

The KHH and KHP parts of the interaction were connected by TBME generated by a potential (H7B) due to Hosaka, Kubo, and Toki [30] plus the Coulomb potential [31] for the pp TBME. The H7B potential is expressed as a superposition of seven one-boson-exchange potentials, the oscillator matrix elements of which were fit to the G-matrix elements derived from the Paris [32] nucleon-nucleon potential. Thus, this is a "bare" interaction with no 1p-1h corrections. However, this may be a better approximation than one might suppose. The 1p-1h renormalization of the KHH and KHP interactions is large and important; but from the only published results for Kuo's calculations of ph TBME, it would seem that the renormalization of this type of matrix element is considerably less. The reason for this would seem to be that the "hole" orbits just below ^{208}Pb are of low spin while the particle orbits just above ^{208}Pb are of high spin so that the overlap between particle and hole orbits is small. This point is illustrated in Table II. Specifically, the average renormalization $\langle \text{abs}(G_{\text{re}})\rangle$ is seen to be 20% of the average Kuo $\langle G_{\text{bare}}\rangle$. For comparison, the average 1p-1h renormalization, $\langle \text{abs}(G_{\text{1p-1h}})\rangle$, is 80% of $\langle \text{abs}(G_{\text{bare}})\rangle$ for the KHH neutron-neutron interaction [26]. Table II also displays the good agreement between the bare TBME of Kuo [33] and of the H7B potential.

The H7B + Coulomb 1p-1h interaction was tested by comparison of calculations for the low-lying odd-parity levels of ^{208}Pb to experiment. In this comparison we assume the spin-parity assignments from the recent work of Maier *et al.* [34]. Experimental information [35] on stripping and pickup spectroscopic factors $\mathcal{S}$, and the g factor of the 5_1^- level of ^{208}Pb at 3198 keV provided stringent tests of the wave functions that result from a delicate balance between neutron and proton 1p-1h excitations. A significant improvement was achieved in the description of the $\mathcal{S}$ and g factors by adding to the H7B + Coulomb interaction a fraction of the Poppelier-Glaudemans SDI interaction. Thus the PKH interaction is given (schematically) by H7B + Coulomb + K_{SDI}·SDI. After a systematic search, a value of $K_{\text{SDI}} = 0.096$ was found to give good agreement with experiment without significantly affecting energy spectra or diagonal TBME, i.e., the principal effect is on the off-diagonal TBME. This then is our "cross-shell" PKH interaction used to join the KHH_e and KHP_e interactions. The PKH interaction alone gives the results reported for $A = 208$ and is the main ingredient in determining the results for $A = 207$ and 209.

III. THE MATRIX ELEMENTS AND THE DECAY RATE

A. Definition of the matrix elements

The nuclear matrix elements which enter into first-forbidden beta decay in the impulse approximation in normal order are formed from the following two classes of operators,

$$\mathbf{r}, [\mathbf{r}, \boldsymbol{\sigma}]^R, \quad R = 0, 1, 2, \tag{3a}$$

$$\gamma_5, \ \boldsymbol{\alpha}, \tag{3b}$$

TABLE II. Selected diagonal two-body-matrix-elements illustrating the degree of agreement between Kuo (Ref. [33]) and the H7B results of Hosaka, Kubo, and Toki (Ref. [30]) for the bare G-matrix TBME (labeled G). The sum of the four renormalizing TBME (labeled G_{re}) listed by Kuo is also included to illustrate the magnitude of the renormalization due to the finite model space.

j_1	j_2	J^π	$\langle j_1 j_2\|V\|j_1 j_2\rangle$		
			G (H7B)	G (KUO)	G_{re} (KUO)
$h_{9/2}$	$p_{1/2}$	4^+	−0.0771	−0.0680	−0.0356
	$p_{1/2}$	5^+	−0.2503	−0.2480	+0.0304
$h_{9/2}$	$f_{5/2}$	2^+	−0.1805	−0.1458	−0.3106
	$f_{5/2}$	3^+	−0.1132	−0.1011	−0.0027
	$f_{5/2}$	4^+	−0.0551	−0.0401	−0.0152
	$f_{5/2}$	5^+	−0.1605	−0.1563	+0.0486
	$f_{5/2}$	6^+	−0.0439	−0.0348	+0.0546
	$f_{5/2}$	7^+	−0.4846	−0.4843	+0.0038
$h_{9/2}$	$p_{3/2}$	3^+	−0.3971	−0.3946	−0.0114
	$p_{3/2}$	4^+	−0.1371	−0.1324	+0.0179
	$p_{3/2}$	5^+	−0.1144	−0.1110	+0.0778
	$p_{3/2}$	6^+	−0.1761	−0.1662	−0.0615
$h_{9/2}$	$i_{13/2}$	2^+	−1.0463	−1.0677	−0.2064
	$i_{13/2}$	3^+	−0.5811	−0.5718	−0.0433
	$i_{13/2}$	4^+	−0.3504	−0.3388	+0.0018
	$i_{13/2}$	5^+	−0.3806	−0.3813	+0.0137
	$i_{13/2}$	6^+	−0.2002	−0.1879	+0.0421
	$i_{13/2}$	7^+	−0.3518	−0.3540	+0.0202
	$i_{13/2}$	8^+	−0.1234	−0.1256	+0.0669
	$i_{13/2}$	9^+	−0.4242	−0.4179	−0.0074
	$i_{13/2}$	10^+	−0.0613	−0.0759	+0.0927
	$i_{13/2}$	11^+	−0.8490	−0.8068	−0.1301
$f_{7/2}$	$p_{1/2}$	3^+	−0.3676	−0.3617	−0.0122
	$p_{1/2}$	4^+	−0.2682	−0.2517	−0.0582
Averages:			−0.2998	−0.2821	0.0569[a]

[a] The average of the absolute values, designated $\langle \text{abs}(G_{\text{re}})\rangle$.

where R is the rank of the operator. The four nonrelativistic operators of Eq. (3a) arise from an expansion of the lepton wave functions, while those of Eq. (3b) occur in the hadronic weak current, connect the large and small components of nucleonic wave functions, and are relativistic. Matrix elements of different rank contribute incoherently to the decay rate. The rank R has the selection rule

$$|J_i - J_f| \leq R \leq |J_i + J_f|. \tag{4}$$

The matrix elements of $\mathbf{r}$, and $\boldsymbol{\alpha}$ are of rank-one while γ_5 is the timelike component of the rank-zero axial current discussed in Sec. I. The conserved-vector-current (CVC) theorem can be invoked to eliminate the matrix element of $\boldsymbol{\alpha}$ via

$$\langle J_f T_f \| \boldsymbol{\alpha}\boldsymbol{\tau} \| J_i T_i \rangle = E_\gamma \langle J_f T_f \| i r C_1 \boldsymbol{\tau} \| J_i T_i \rangle \tag{5}$$

where $C_L = [4\pi/(2L+1)]^{1/2} Y_L$. For β^- decay, E_γ is the energy separation (natural units) in the final nucleus between the initial state's analog and the final state. For $A = 205$–212 it is well represented by [36]

$$E_\gamma = \frac{1.412}{0.511}\left(\frac{Z_i + Z_f}{2A^{\frac{1}{3}}}\right) - 0.811 - 0.782 + Q(\beta^-). \tag{6}$$

We expect Eq. (5) to hold to a high accuracy in the lead region (relative to lighter nuclei) just because E_γ is larger here and its uncertainty is roughly independent of A. We thus have five independent matrix elements: two each of rank-zero ($R0$) and rank-one ($R1$) and one of rank-two ($R2$) which we denote as

$$\begin{aligned} R0: &\quad M_0^S,\ M_0^T, \\ R1: &\quad M_1^x,\ M_1^u, \\ R2: &\quad M_2^z, \end{aligned} \tag{7}$$

where α of M_R^α is S, u, and z for the $R = 0,1,2$ operators of $[\mathbf{r}, \boldsymbol{\sigma}]^R, T$ for γ_5, and x for $\mathbf{r}$. The notation for the $R0$ matrix elements is intended to remind us that they are the matrix elements of the space-like and time-like components of the axial current. The notation for the R1 and R2 values symbols are historical [37].

The evaluation of these matrix elements is made via Eq. (1). There are three steps: (1) the evaluation of single-particle matrix elements $M_R^\alpha(j_i j_f)$, (2) the evaluation of the quenching factors $q_\alpha(j_i j_f)$, and (3) the combining of these quantities with the $D_R(j_i j_f)$ to form the $\mathcal{M}_R^\alpha(j_i j_f)$ and finally M_R^α. We consider the first two of these steps in the next two subsections. The final step will be discussed in Sec. IV after we first describe how the matrix elements are combined to form the decay rate and other observables.

B. The evaluation of the $M_R^\alpha(j_i j_f)$

The single-particle matrix elements $M_R^\alpha(j_i j_f)$ were evaluated using Woods-Saxon (WS) radial wave functions with the parameters of Streets, Brown, and Hodgson [38]. These parameters reproduce the experimental rms charge radius of ^{208}Pb of 5.503(2) fm and give a neutron rms radius 0.2 fm larger. With normal shell occupancies, these radii correspond to harmonic-oscillator (HO) parameters of $\hbar\omega = 6.701$ and 7.183 MeV for protons and neutrons, respectively. If the $M_R^\alpha(j_i j_f)$ are evaluated with HO wave functions with $\hbar\omega$ equal to the average of the neutron and proton values, then the results are usually close to those obtained with Woods-Saxon wave functions. The exceptions involve those transitions between single-particle states with zero and one node, respectively. For example, $\nu 1g_{9/2} \rightarrow \pi 0h_{9/2}$ for which the integrals have two contributions which are opposite in sign but nearly equal in magnitude.

The $M_R^\alpha(j_i j_f)$ evaluated with Woods-Saxon radial wave functions are dependent on the separation energies of the active orbits. The question arises as to how to handle this dependence when the parentage of the orbits is fractionated. We now address this question with $R0$ decays chosen to illustrate the approach.

For $R0$ matrix elements the single-particle transitions are constrained by $j_i = j_f \equiv j$. Thus Eq. (1) simplifies to

$$M_0^S = \sum_j D_0(j) q_S(j) M_0^S(j) \tag{8}$$

with a similar relationship for M_0^T. Strictly speaking, Eqs. (1) and (8) are correct only in as far as the $M_R^\alpha(j_i j_f)$ and $D_R(j_i j_f)$ have no nuclear structure dependencies in common. For spin-zero initial and final states the $D_R(j)$ can be formulated by

$$D_0(j) = \sum_i D_0(j,i) = (2j+1)^{-\frac{1}{2}} \sum_i \mathcal{A}_n(j,i)\mathcal{A}_p(j,i), \tag{9}$$

where j simultaneously specifies the possible single-particle transitions and the spin of the common $A-1$ core states which are labeled for given j by the index i. These core states have the spectroscopic amplitudes $\mathcal{A}_n(j,i)$ and $\mathcal{A}_p(j,i)$ for the initial and final states of the β^- decay, respectively. The spectroscopic factor $\mathcal{S}$ is the square of $\mathcal{A}$ which is reduced in both J and T. The spectroscopic factors satisfy the sum rules

$$\sum_i \mathcal{S}_n(j,i) = \overline{n}(j), \qquad \sum_i \mathcal{S}_p(j,i) = \overline{p}(j), \tag{10}$$

where $\overline{n}(j)$ [$\overline{p}(j)$] is the mean number of neutrons [protons] in orbit j of the initial [final] state of the β decay.

For realistic radial wave functions such as the Woods-Saxon or Hartree-Fock forms, the radial integrals of $M_0^S(j)$ and $M_0^T(j)$ are dependent on the neutron and proton separation energies of the active nucleons and thus depend on the nuclear structure of the initial and final states. Millener [12] formulated a prescription for dealing with this dependence which, for present purposes, follows from Eqs. (9)–(10):

$$M_0^S = \sum_{j,i} (2j+1)^{-\frac{1}{2}} \mathcal{A}_n(j,i)\mathcal{A}_p(j,i) q_S(j) M_0^S(j,i), \tag{11}$$

where a specific proton and neutron separation energy

is associated with the index i. A simple and revealing method of utilizing Eqs. (8)–(11) is to make use of the fact that the neutron and proton separation energies depend linearly on the excitation energy, $E_x(j,i)$, of the ith state of spin j in the $A-1$ nucleus. Thus $M_0^S(j)$ and $M_0^T(j)$ can be expressed as power series in the $E_x(j,i)$ and are therefore given in terms of energy moments weighed by the $\sum_i D_R(j,i)$ of Eq. (9). It is found that a linear dependence on $E_x(j,i)$ is adequate for present purposes, i.e.,

$$M_0^S(j,i) = M_0^S(j,1)\left\{1+\delta_S\left[E_x(j,i)-E_x(j,1)\right]\right\}, \tag{12}$$

so that with

$$\langle E_{xj}\rangle = \frac{\sum_i \mathcal{A}_n(j,i)\mathcal{A}_p(j,i)E_x(j,i)}{\sum_i \mathcal{A}_n(j,i)\mathcal{A}_p(j,i)} - E_x(j,1) \tag{13}$$

we have

$$M_0^S(j) = M_0^S(j,1)\left\{1+\delta_S\langle E_{xj}\rangle\right\} \tag{14}$$

with a similar expression for $M_0^T(j)$.

In order to use this approach the energy spectra and wave functions of the $\frac{1}{2}^-$, $\frac{3}{2}^-$, $\frac{5}{2}^-$, $\frac{9}{2}^+$, and $\frac{11}{2}^+$ states of ^{205}Hg, and the $\frac{1}{2}^+$, $\frac{3}{2}^+$, $\frac{5}{2}^+$, $\frac{9}{2}^-$, and $\frac{11}{2}^-$ states of ^{205}Tl were calculated and the $\mathcal{A}_n(j,i)$ and $\mathcal{A}_p(j,i)$ for $i=1,20$ were extracted for both ^{206}Hg and ^{206}Tl decay. The same calculation was made for the $\frac{9}{2}^+$ and $\frac{11}{2}^+$ states of ^{209}Pb for use with ^{210}Pb$(0^+) \rightarrow {}^{210}Bi(0^-)$. Details of these calculations and their application to Eqs. (8) and (14) are given in Appendix A. Results are summarized in Table III. This table illustrates that the dependence of the M_0^S and M_0^T on the separation energies is negligible. We note that this result is contrary to what might have been inferred from arguments put forth by Millener, Warburton, and colleagues [39, 12], who displayed figures emphasizing the strong dependence of the $R0$ matrix elements on $S(p)$ and $S(n)$ but left as implicit the relationship between $S(p)$ and $S(n)$ given by their definitions:

$$S(p) - S(n) = Q(\beta^-) - 0.782 \text{ MeV}. \tag{15}$$

When this relationship is used, the dependence of the ma-

TABLE III. Evaluation of the $M_0^S(j)$ and $M_0^T(j)$ of Eqs. (8) and (14). The number in brackets in columns 5 and 6 is the power of ten.

j	$M_0^S(j;1)$ (fm)	$M_0^T(j;1)$ (fm)	$\langle E_{xj}\rangle$ MeV	$\delta_S\langle E_{xj}\rangle$	$\delta_T\langle E_{xj}\rangle$	$M_0^S(j)$ (fm)	$M_0^T(j)$ (fm)
			^{206}Hg → ^{206}Tl				
$\frac{1}{2}$	+8.212	−104.0	+0.165	−7.82[−4]	+8.41[−4]	+8.206	−104.1
$\frac{3}{2}$	−8.069	+124.7	−1.461	+6.10[−3]	−4.65[−3]	−8.119	+124.1
$\frac{5}{2}$	+16.38	−196.2	−11.689	+5.60[−2]	−2.71[−2]	+17.30	−190.9
$\frac{9}{2}$	−7.076	+172.2	+0.620	−4.50[−3]	+3.90[−3]	−7.044	+172.9
$\frac{11}{2}$	+26.11	−366.3	+0.030	−9.87[−5]	+9.57[−5]	+26.10	−366.3
			^{206}Tl → ^{206}Pb				
$\frac{1}{2}$	+8.179	−104.6	+0.224	−8.96[−4]	+1.05[−3]	+8.172	−104.7
$\frac{3}{2}$	−8.012	+125.4	−3.677	+1.38[−2]	−1.10[−2]	−8.123	+124.0
$\frac{5}{2}$	+16.33	−198.1	−5.511	+2.52[−2]	−1.14[−2]	+16.74	−195.8
$\frac{9}{2}$	−6.980	+173.8	+1.063	−5.14[−3]	+4.39[−3]	−6.944	+174.6
$\frac{11}{2}$	+26.21	−366.0	−0.116	+3.95[−4]	−2.59[−4]	+26.22	−365.9
			^{209}Pb → ^{209}Bi				
$\frac{9}{2}$	−7.417	+164.8	+0.245	−1.51[−3]	+1.46[−3]	−7.406	+165.1
$\frac{11}{2}$	+26.81	−358.9	+0.947	−3.73[−3]	+2.31[−3]	+26.71	−359.7

trix elements on separation energy in the $A = 16$ region is reduced over that explicitly displayed [12]. However, it is still larger near $A = 16$ than in the lead region, e.g., the results of Table III, simply because at $A \approx 208$, $S(n)$ is considerably larger, and $S(n)$ and $S(p)$ are more nearly equal.

Because of the insensitivity to $S(n)$ and $S(p)$ illustrated here, we evaluate the matrix elements of all ranks assuming a single parent in the $A - 1$ nucleus. However, the excitation energy of this parent was chosen after consideration of the shell-model results so as to minimize the error introduced by this approximation.

C. Core polarization and effective operators

First-order contributions from excitations of the core can have a large effect on the first-forbidden matrix elements [40]. The important core-excited admixtures in the initial (final) state are those connected by a one-body operator to the dominant terms in the final (initial) state wave function. A schematic of typical configurations involved is shown in Fig. 3. Restrictions on the matrix elements of $\mathbf{r}$ and its derivatives effectively limits first-forbidden decay to transitions between adjacent major shells. This selection rule (exact for HO wave functions) and Pauli blocking due to the large neutron excess severely restricts the contributions from initial-state admixtures for the lead region. For the decays considered here, only those involving $0h_{11/2}$ proton holes contribute and — with the exception of the rank-two $\nu 1g_{7/2} \rightarrow \pi 0h_{11/2}$ transition — all are included in the PKH model

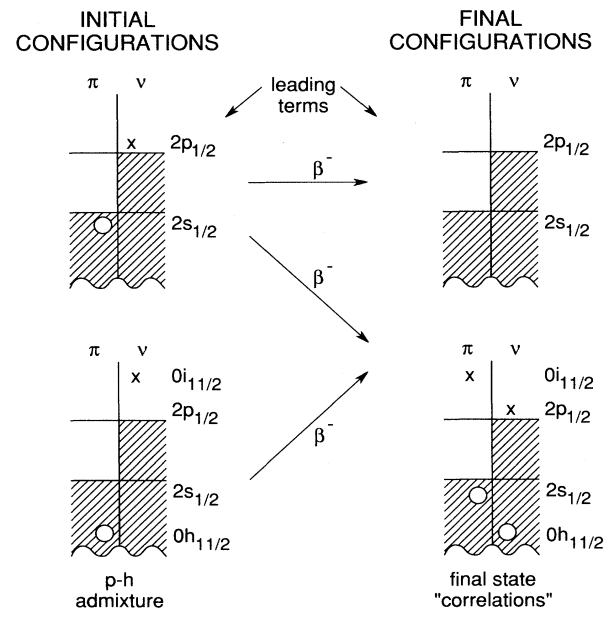

FIG. 3. Schematic illustrating the role in first-forbidden β^- decay of 1p-1h admixtures in the initial state and 2p-2h "correlations" in the final state. Arrows indicate the configurations linked by the β^- decay. The example shown is specific to $^{206}\mathrm{Tl} \rightarrow {}^{206}\mathrm{Pb}$.

space and thus need not be added perturbatively. This is just as well, since the energy denominators for these initial-state admixtures are not always large or constant enough to render the perturbative result accurate in all cases.

Specifying the major shell by the quantum number Q [$Q = 2n + l$, where n is the principal quantum (= 0,1,...) and l is the orbital angular momentum], there are many possible $\Delta Q = \pm 1$ transitions involving the 2p-2h admixtures in the final state. Those affecting the allowable transitions from the neutron-hole states of the PKH model space were considered in a recent treatment of core polarization in the lead region [40]. These results give explicit values for the $q_\alpha(j_i j_f)$ of Eq. (1) derived using the H7B interaction discussed in Sec. II C. We use the results obtained with Woods-Saxon wave functions. For the present application we also need $q_\alpha(j_i j_f)$ for the allowable β^- single-particle transitions commencing from the neutron-particle orbits of Fig. 2. These $q_\alpha(j_i j_f)$ were calculated with the H7B interaction and Woods-Saxon radial wave functions by the procedures of Ref. 40 and are listed in Table IV.

D. The Behrens-Bühring expansion

1. Introduction

In this subsection we delineate the relationship between the β decay rate and the nuclear matrix elements contributing to it. Although the approach used has been fully discussed previously [13], it was not used by the present author for nuclei heavier than ^{96}Y [14] and an examination of its applicability to the lead region is in order. We follow the Behrens-Bühring [41, 19] formulation. In this formulation the beta decay formulas are derived by expanding the electron radial wave functions in powers of the mass and energy parameters of the electron and of the nuclear charge and size via the products αZ, $W r_u$, $p r_u$, and $q r_u$ where W and p are the electron energy and momentum and q is the neutrino momentum. In this treatment additional matrix elements occur which contain both the nuclear and electromagnetic structure of the nucleus via the shape of the nuclear charge distribution. The use of a uniform charge distribution of radius r_u is a very good approximation provided it implies the correct experimental rms size of the nucleus. We use for r_u the expression given by Brown *et al.* [42]. The additional $R0$ and $R1$ matrix elements needed are obtained from the definitions of M_0^S, M_1^x, and M_1^u by including in the radial integrals an extra factor [41]

$$\frac{2}{3} I(1,1,1,1;r) = \left[1 - \frac{1}{5}\left(\frac{r}{r_u}\right)^2\right] \qquad 0 < r < r_u$$
$$= \left[\frac{r_u}{r} - \frac{1}{5}\left(\frac{r_u}{r}\right)^3\right] \qquad r > r_u \qquad (16)$$

and are denoted $M_0^{S\prime}$, $M_1^{x\prime}$, and $M_1^{u\prime}$. We shall use as variables, M_0^S, M_1^x, M_1^u, r'_w ($\equiv M_0^{S\prime}/M_0^S$), r'_x ($\equiv M_1^{x\prime}/M_1^x$), r'_u ($\equiv M_1^{u\prime}/M_1^u$), and M_2^z.

It was found that the terms generated by the next order in the Behrens-Bühring expansion were negligible for all cases encountered in the $A \sim 16$, 40, and 96 regions [12, 13]. However for $A \sim 208$ it is desirable to make a careful assessment of higher-order terms, especially those generated by the power series in αZ since this parameter is 0.61 for, e.g., ^{210}Pb β^- decay (as opposed to ≤ 0.019 for $W_0 r_u$). This assessment has been made for $R0$ decays since these are our major interest [43]. All second-order terms and several third-order terms were considered and were found to be small compared to M_0^S, M_0^T, and $M_0^{S'}$. They will have a noticeable effect on the $R0$ β decay rate only if there is strong cancellation between the three first-order terms and the very low $f_0 t$ values for the decays under consideration here show that this cancellation cannot be strong. Higher-order terms are large enough to influence the shape factor, and, in fact, Wiesner *et al.* [45, 46] obtained an experimental verification of the combined effect of these terms from a careful measurement of the shape factor for the ^{206}Hg(0^+) $\rightarrow$ ^{206}Tl(0^-) transition. The role of higher-order rank-zero terms is summarized in Appendix B.

TABLE IV. The first-order perturbative quenching factor $q_\alpha(j_i j_f)$ calculated for $Q = 6 \rightarrow Q = 5$ transitions with WS radial matrix elements and the H7B residual interaction. The results are valid for a final state with $Z \leq 82$, $N \geq 126$.

Matrix element	Orbit ν	Orbit π	$q_\alpha(j_i j_f)$	Δ_n[a]
M_0^S	$0i_{11/2}$	$0h_{11/2}$	0.8426	+0.0333
	$1g_{9/2}$	$0h_{9/2}$	1.2856	−0.0723
	$1g_{7/2}$	$1f_{7/2}$	0.8512	+0.0196
	$2d_{5/2}$	$1f_{5/2}$	1.1388	−0.0088
	$2d_{3/2}$	$2p_{3/2}$	0.9017	+0.0348
	$3s_{1/2}$	$2p_{1/2}$	0.9782	+0.0183
M_0^T	$0i_{11/2}$	$0h_{11/2}$	1.1520	−0.0319
	$1g_{9/2}$	$0h_{9/2}$	0.8317	+0.0399
	$1g_{7/2}$	$1f_{7/2}$	1.1472	−0.0200
	$2d_{5/2}$	$1f_{5/2}$	0.8963	+0.0076
	$2d_{3/2}$	$2p_{3/2}$	1.1025	−0.0371
	$3s_{1/2}$	$2p_{1/2}$	0.9870	−0.0180
M_1^u	$0i_{11/2}$	$0h_{11/2}$	0.6001	+0.0655
	$0i_{11/2}$	$0h_{9/2}$	0.3102	+0.2088
	$1g_{9/2}$	$0h_{11/2}$	0.6636	−0.0416
	$1g_{9/2}$	$0h_{9/2}$	0.4683	−0.0420
	$1g_{9/2}$	$1f_{7/2}$	0.3596	+0.0811
	$1g_{7/2}$	$0h_{9/2}$	0.5957	+0.0963
	$1g_{7/2}$	$1f_{7/2}$	0.5241	+0.0947
	$1g_{7/2}$	$1f_{5/2}$	0.3295	+0.1740
	$2d_{5/2}$	$1f_{7/2}$	0.5946	+0.1019
	$2d_{5/2}$	$1f_{5/2}$	0.5668	+0.0717
	$2d_{5/2}$	$2p_{3/2}$	0.4728	+0.0427
	$2d_{3/2}$	$1f_{5/2}$	0.5993	+0.0351
	$2d_{3/2}$	$2p_{3/2}$	0.5401	+0.0986
	$2d_{3/2}$	$2p_{1/2}$	0.4340	+0.1503
	$3s_{1/2}$	$2p_{3/2}$	0.5581	+0.1279
	$3s_{1/2}$	$2p_{1/2}$	0.5602	+0.0701
	$0j_{15/2}$	$0i_{13/2}$	0.4259	+0.0469
M_1^x	$0i_{11/2}$	$0h_{11/2}$	0.5942	+0.3431
	$0i_{11/2}$	$0h_{9/2}$	0.5936	+0.1572
	$1g_{9/2}$	$0h_{11/2}$	0.7874	−0.0354
	$1g_{9/2}$	$0h_{9/2}$	0.9899	+0.3911
	$1g_{9/2}$	$1f_{7/2}$	0.5957	+0.0004
	$1g_{7/2}$	$0h_{9/2}$	0.6378	−0.0023
	$1g_{7/2}$	$1f_{7/2}$	0.5707	+0.3468
	$1g_{7/2}$	$1f_{5/2}$	0.5633	+0.1010
	$2d_{5/2}$	$1f_{7/2}$	0.7896	+0.0760
	$2d_{5/2}$	$1f_{5/2}$	0.8723	−0.0227
	$2d_{5/2}$	$2p_{3/2}$	0.7003	+0.0257
	$2d_{3/2}$	$1f_{5/2}$	0.7801	+0.0748
	$2d_{3/2}$	$2p_{3/2}$	0.6843	+0.1975
	$2d_{3/2}$	$2p_{1/2}$	0.6721	+0.1136
	$3s_{1/2}$	$2p_{3/2}$	0.7888	+0.0991
	$3s_{1/2}$	$2p_{1/2}$	0.8255	+0.0206
	$0j_{15/2}$	$0i_{13/2}$	0.6668	+0.0164

[a] For occupancy of the $\nu 1g_{9/2}$ orbit in the initial state by $n(1g_{9/2})$ neutrons, $q_\alpha(j_i j_f)$ is given by the value listed minus $\sqrt{n(1g_{9/2})/10}\Delta_n$.

2. *Construction of the decay rate*

Past usage relates experimental and theoretical decay rates via

$$ft = 6166, \tag{17}$$

where

$$f = \int_1^{W_0} C(W) F(Z,W) (W^2-1)^{1/2} W (W_0 - W)^2 dW \tag{18}$$

and t is the partial half-life of the transition. In Eq. (18) $C(W)$ is the shape factor, $F(Z,W)$ is the Fermi function, W is the electron energy, and W_0 is the total disintegration energy — both including the rest mass — and all quantities are in natural units $\hbar = c = m_e = 1$. The unit of time is the second and of length the electron Compton wavelength, $\lambda_{Ce} = 386.159$ fm. With dominant terms retained, the shape factor can be expressed as [37, 19, 13]

$$C(W) = k + kaW + kb/W + kcW^2. \tag{19}$$

A more directly pertinent observable than f is the decay rate:

$$\Lambda(\text{sec}^{-1}) = 1/\tau = \ln 2/t = f/8896. \tag{20}$$

The integrated Fermi function for allowed decays is

$$f_0 = \int_1^{W_0} F(Z,W)(W^2-1)^{1/2} W (W_0 - W)^2 dW. \tag{21}$$

The Wilkinson-Macefield [47] parametrization of f_0 is used to evaluate Eq. (21). Some remarks on the accuracy of this evaluation are given in Appendix C. The integral in Eq. (18) has four terms corresponding to the four terms in $C(W)$ of Eq. (19). For the first term we use f_0. The other three terms are evaluated by numerical integration. Behrens and Bühring [19] define the averaged shape factor by

$$\overline{C(W)} = f/f_0 \tag{22}$$

in terms of which experiment and theory for n-forbidden β decay can be related via

$$\overline{C(W)}(\mathrm{fm}^{2n}) = \frac{6166\lambda_{Ce}{}^{2n}}{f_0 t} \quad (n \text{ forbidden}) \tag{23}$$

For convenience, we choose to give the first-forbidden matrix elements in fm rather than natural units, hence for first-forbidden decays $\overline{C(W)}$ is in fm^2 and is given by

$$\overline{C(W)}(fm^2) = \frac{9195 \times 10^5}{f_0 t} \quad (\text{1st forbidden}) \tag{24}$$

For allowed (Gamow-Teller) decays $\overline{C(W)}$ is just the square of the Gamow-Teller matrix element of $\boldsymbol{\sigma\tau}$ which we term the Gamow-Teller beta-moment $B_0^{(1)}$. First-forbidden decays are incoherent in the rank so that $\overline{C(W)}$ can be expressed as the sum of the $R0$, $R1$, and $R2$ contributions, i.e.,

$$\overline{C(W)} = B_1^{(0)} + B_1^{(1)} + \tfrac{1}{3}\overline{q^2 + \lambda_2 p^2} B_1^{(2)} \tag{25}$$

where n in $B_n^{(R)}$ denotes the degree of forbiddeness. Equation (25) should be regarded as a definition of the $B_n^{(R)}$: it does not imply that $R0$ and $R1$ first-forbidden decays have allowed shapes, i.e., see Eq. (19). Our evaluation of $\overline{C(W)}$, or alternately the $B_1^{(R)}$, follows the procedures outlined by Warburton *et al.* [13] and previously applied to $Z \leq 40$ decays. The expressions used to calculate the $B_1^{(R)}$ contain the Coulomb functions [19] μ_1 and λ_2. These were assumed to be constant at unity in applications to $Z \leq 40$. In the lead region, this is still a fairly good approximation for μ_1 for the decay energies of interest here ($|\mu_1 - 1| \leq 0.06$). However, for $Z \sim 82$, λ_2 deviates considerably from unity [19]. It transpires that for the $R0$ and $R1$ components of the decay, the terms proportional to these Coulomb functions are relatively very small and the assumption that $\mu_1 = \lambda_2 = 1$ generates <0.3% error in the decay rates considered here. Therefore, we retain this assumption in deriving the $R0$ and $R1$ contributions. This insensitivity to λ_2 follows from the dominance at high Z of those first-forbidden terms which are proportional to Z: these terms do not depend on μ_1 or λ_2. The atomic number Z is contained in $\xi = \alpha Z/2r_u$. The "ξ approximation" ($\xi \equiv$ xi) is the expression used to describe calculations in which only the terms proportional to ξ are retained [19]. The $R2$ shape factor,

$$C(W)_{\text{unique}} = \tfrac{1}{3}B_1^{(2)}[q^2 + \lambda_2 p^2], \tag{26}$$

is not proportional to Z and thus is normally negligible for $\Delta J = 0$ or 1 decays for $Z \sim 82$. In fact, it is negligible for all cases considered here. However, it is clear from Eq. (26) that $\Delta J = 2$ decays are sensitive to λ_2. For these $R2$ decays we extract the experimental beta-moment $B_1^{(2)}$ [$\equiv \frac{1}{4}(M_2^z)^2$] using the results of Gove and Martin [48] for $\log[\overline{C(W)}]$ since Gove and Martin treat all Coulomb terms with adequate accuracy. The dominance of the ξ terms for $R0$ and $R1$ decays in the lead region allows approximations, which are useful for displaying the dependence of the rates on the matrix elements. If we retain just the $R0$ term ζ_0^2 ($\zeta \equiv$ zeta) and the $R1$ term ζ_1^2 contained in the energy-independent term k of Eq. (19) and described in Eqs (30)–(31) of Ref. 13, we have

$$B_1^{(0)} = [M_1^{(0)}]^2 = [\epsilon_{\text{mec}} M_0^T + a_S M_0^S]^2,$$
$$B_1^{(1)} = [M_1^{(1)}]^2 = [a_u M_1^u - a_x M_1^x]^2 \tag{27}$$

(ζ approximation),

where

$$\begin{aligned} a_S(Z, W_0, r_u) &= r'_w \xi + \tfrac{1}{3}W_0, \\ a_u(Z, W_0, r_u) &= r'_u \xi - \tfrac{1}{3}W_0, \\ a_x(Z, W_0, r_u) &= E_\gamma - r'_x \xi - \tfrac{1}{3}W_0. \end{aligned} \tag{28}$$

In the ζ approximation the decays have the allowed shape. Note that this is different than the "ξ approximation" because some terms not proportional to Z are retained. A more important difference is that in the full expansion for the $R1$ component there is a contribution from the ka term of Eq. (19) which is proportional to ξ. This term is ~10% of the k term and, logically should be retained in the ξ approximation although it is often not. In any case, because this term is neglected, the ζ approximation for $R1$ decays has an error of ~10% for Z ~82 while for $R0$ decays all terms in ξ are retained but the neglect of the kb/W term of Eq. (19) causes an error of ~4% (see Appendix B).

From now on we will explicitly display the expected enhancement of M_0^T over the impulse approximation by means of the meson-enhancement-contribution (mec) parameter ϵ_{mec} as in Eq. (27). For HO wave functions $M_0^T(j_i j_f)$ and $M_0^S(j_i j_f)$ are related by [13]

$$M_0^T(j_i j_f) = -\left[\frac{E_{\text{osc}}}{m_e c^2}\right] M_0^S(j_i j_f). \tag{29}$$

Using Eq. (29) with $E_{\text{osc}} = \hbar\omega = 7$ MeV and $a_S \approx 14$, and neglecting the quenching factors $q_{S,T}(j_i j_f)$ which are close to unity for $R0$ decays, we have

$$B_1^{(0)} \approx [14\epsilon_{\text{mec}} - 14]^2 (M_0^S)^2$$

(ζ and HO approximations). (30)

It is immediately clear from this approximate result why the observation of fast $R0$ decays calls for strong mec effects. The parameters a_u and a_x are rather constant for the $R1$ decays we will consider. A typical case is $^{206}\mathrm{Hg}(0^+) \rightarrow {}^{206}\mathrm{Tl}(1^-)$ for which

$$B_1^{(1)} \approx [12.1 M_1^u - 22.2 M_1^x]^2 \quad (\zeta \text{ approximation}). \tag{31}$$

On the average $|M_1^u| \sim 2|M_1^x|$ so that the $R1$ decay rate depends critically on the relative sign of M_1^u and M_1^x which varies with j_i and j_f.

To summarize, we choose to present our comparison of experiment and theory via Eqs. (24) and (25). Specifi-

cally we will give experimental and theoretical values of $\log f_0 t$ and $\overline{C(W)}^{1/2}$ (in fm) which are related by this equation. If the decay is pure $R0$ or $R1$, $\overline{C(W)}^{1/2}$ is equivalent to $M_1^{(0)}$ or $M_1^{(1)}$, respectively [see, e.g., Eq. (27)]. Otherwise it is the square root of the sum of the allowable beta moments. We display Eq. (27) for pedagogical reasons; our results do not rely on either the ξ or ζ approximation.

IV. EFFECTIVE OPERATORS DETERMINED FROM A LEAST-SQUARES FIT

A. The shell-model calculation

We have described all the ingredients of Eq. (1) and have explained how to combine the matrix elements to obtain a theoretical decay rate or values for f, $f_0 t$, or $\overline{C(W)}^{1/2}$. We shall give some specific examples of the shell-model calculations of the $D_R(j_i j_f)$ of Eq. (1) in the next subsection where we discuss specific decays. In general the shell-model results for the D_R included input from two calculations: (1) either the KHH_e interaction ($A = 205$–206), or the KHP_e interaction ($A = 210$–212), and (2) all 1p-1h excitations across the $Z = 82$, $N = 126$ interface of both the initial and final states with the PKH interaction. For A =207, 208, and 209 the transitions of interest are either non-existent or trivial in the KHH or KHP model spaces and only the PKH calculation was made. The J dimensions of the PKH calculations varied from 24 for the $\frac{1}{2}^+$ states of ^{207}Tl to 2538 for the $\frac{1}{2}^+$ states of ^{205}Tl. The calculations for ^{211}Pb and ^{212}Pb decay involved rather large J dimensions in the KHP model space and a full 1p-1h calculation was not possible. In these two cases the important $\nu 0i_{11/2} \rightarrow \pi 0h_{11/2}$ and $\nu 1g_{9/2} \rightarrow \pi 0h_{11/2}$ 1p-1h contributions were determined perturbatively by diagonalizing in a highly-truncated PKH model space containing only the very basic ingredients contributing to the decays. That this method was accurate was verified by repeating the 1p-1h calculations for $A = 206$ and 210 with the same highly truncated model space and thereby demonstrating good agreement of the $D_R(j_i j_f)$ with those obtained with the full model space.

A major part of the calculations were repeated with the SDI interaction of Poppelier and Glaudemans [21]. However, the Coulomb energy was not treated consistently in the derivation of this interaction so that, e.g., it cannot be used for the ^{208}Tl decays (Fig. 1) since the wave functions of the ^{208}Pb 1p-1h states depend sensitively on the relative energies of proton and neutron excitations. Also its single-particle energies will be somewhat distorted. Thus we concentrate our attention on the results using the KHH and PKH interactions, but sometimes use the SDI interaction for comparison or ancillary calculations.

It is our assumption that the matrix elements contributing to the first-forbidden decay rates are all fairly well determined with the exception of the two-body (mec) contribution to the matrix element of γ_5. Thus our procedure is (1) to calculate the one-body matrix elements, including the core-polarization corrections, as accurately as possible, (2) to combine these to obtain the $R0$ and $R1$ beta moments, and then to perform a least-squares fit to

$$\overline{C(W)}^{1/2} = [B_1^{(0)}(\epsilon_{\mathrm{mec}}) + B_1^{(1)}(sq_x, sq_u)]^{1/2} \qquad (32)$$

where the quantities varied in the fit are explicitly displayed as variables and sq_x and sq_u are scaling factors multiplying M_1^x and M_1^u and assumed to be orbit and state independent. The fit was made to the eighteen decays for $A = 205$–212 shown in Fig. 1. The shape factor for the $^{207}\mathrm{Tl}(\frac{1}{2}^+) \rightarrow {}^{207}\mathrm{Pb}(\frac{1}{2}^-)$ decay [45] was also included in the fit. It was found that the individual $R1$ scaling factors were poorly determined and highly dependent on the theoretical uncertainty assumed in the fit. It is more meaningful to assume an overall $R1$ scaling factor via

$$\overline{C(W)}^{1/2} = [B_1^{(0)}(\epsilon_{\mathrm{mec}}) + B_1^{(1)}(sq_1)]^{1/2} \qquad (33)$$

with $sq_1 \equiv sq_x = sq_u$. The result of the fit to Eq. (33) was $\epsilon_{\mathrm{mec}} = 2.01 \pm 0.05$, $q_1 = 0.97 \pm 0.06$, and χ^2_D (chi-squared-per-degree-of-freedom) = 1.00 if a uniform uncertainty of 13% is ascribed to the calculation of all eighteen $\overline{C(W)}^{1/2}$, or, alternatively, if an uncertainty in $\overline{C(W)}^{1/2}$ of $0.07\overline{C(W)}^{1/2} + 3.2$ fm is assumed. From past experience we know that the latter is more meaningful since the weaker decays have larger fractional uncertainties. [With this latter theoretical uncertainty, a least-squares fit to Eq. (32) yields $\epsilon_{\mathrm{mec}} = 2.01 \pm 0.05$, $sq_x = 1.10 \pm 0.18$, and $sq_u = 0.75 \pm 0.20$.] The results of the fit to Eq. (33) are summarized in Fig. 4 and Table V. An important question is just how sensitive is the result to the specific shell-model interaction used to obtain it. The result obtained for ϵ_{mec} with the SDI interaction for all decays of Table V except those for $A = 208$ was consistent with the result of $\epsilon_{\mathrm{mec}} = 2.01$ but with a larger spread in individual values (a least-squares fit was not performed). It is clear that the parametrization of Eq. (33) results in a highly successful description of the decays of Table V and Fig. 4. The possible significance of the values obtained for ϵ_{mec} and sq_1 will be discussed in Sec. VI. But first we will consider the decays of Table V and some others as well.

B. Discussion of the specific decays

The eighteen decays under consideration show a great deal of regularity and can be qualitatively understood with rather simple ideas. As an aid to this understanding a calculation was made of the $(M_0^S)^2$, $(M_1^u)^2$, and $(M_1^x)^2$ transition strength distributions connecting ^{206}Tl 0^- and 1^- states with the ^{206}Pb 0^+ ground state. The calculation was done in the PKH model space with all possible 1p-1h excitations of the initial and final states included. There are 114 0^+, 185 0^- and 514 1^- states in the diagonalization. The strength distribution for these 0^- and 1^- states is shown in Fig. 5. The distributions have been folded with a Gaussian resolution function for ease of viewing and to simulate experimental spectra for

TABLE V. Results of a least-squares fit to eighteen decay rates and one shape factor. The last column gives the percentage of the decay rate due to rank zero.

Transition		E_x	$\log f_0 t$		$\overline{C(W)}^{1/2}$		Δ_m[a]	$B_1^{(0)}$
Initial	Final	(keV)	expt.	theory	expt.	theory	(%)	(%)
^{205}Hg($\frac{1}{2}^-$)	^{205}Tl($\frac{1}{2}^+$)	0	5.274(12)	5.307	69.9(9)	67.3	3.7	45.6
^{206}Hg(0^+)	^{206}Tl(0^-)	0	5.42(9)	5.173	59.4(59)	78.6	−32.1	100.0
^{206}Hg(0^+)	^{206}Tl(1^-)	305	5.23(9)	5.181	73.6(72)	77.9	−5.8	0.0
^{206}Tl(0^-)	^{206}Pb(0^+)	0	5.184(5)	5.270	77.4(2)	70.3	9.1	100.0
^{207}Tl($\frac{1}{2}^+$)	^{207}Pb($\frac{1}{2}^-$)	0	5.128(7)	5.119	82.7(2)	83.6	−1.2	38.1
^{208}Tl(5^+)	^{208}Pb(5^-)	3198	5.619(11)	5.705	46.8(6)	42.6	9.1	40.8
^{208}Tl(4^+)	^{208}Pb(4^-)	3475	5.700(9)	5.591	42.9(4)	48.5	−13.2	0.0
^{208}Tl(5^+)	^{208}Pb(5^-)	3708	5.379(12)	5.327	61.7(8)	65.8	−6.7	76.0
^{209}Tl($\frac{1}{2}^+$)	^{209}Pb($\frac{1}{2}^-$)	2152	5.189(17)	5.068	77.1(12)	88.7	−15.0	46.4
^{209}Pb($\frac{9}{2}^+$)	^{209}Bi($\frac{9}{2}^-$)	0	5.544(3)	5.664	51.3(1)	44.7	13.0	99.0
^{210}Pb(0^+)	^{210}Bi(1^-)	0	7.827(66)	7.838	3.7(3)	3.7	1.3	0.0
^{210}Pb(0^+)	^{210}Bi(0^-)	47	5.468(43)	5.567	55.9(10)	49.9	10.7	100.0
^{211}Pb($\frac{9}{2}^+$)	^{211}Bi($\frac{9}{2}^-$)	0	6.015(7)	6.096	29.8(15)	27.1	8.9	95.0
^{211}Pb($\frac{9}{2}^+$)	^{211}Bi($\frac{9}{2}^-$)	832	5.754(19)	5.828	40.3(20)	37.0	8.2	99.8
^{211}Pb($\frac{9}{2}^+$)	^{211}Bi($\frac{9}{2}^-$)	1109	5.627(37)	5.597	46.6(23)	48.2	−3.4	99.7
^{212}Pb(0^+)	^{212}Bi(1^-)	0	6.809(90)	7.130	11.9(12)	8.3	31.0	0.0
^{212}Pb(0^+)	^{212}Bi(0^-)	239	5.190(20)	5.234	77.0(11)	73.2	5.0	100.0
^{212}Pb(0^+)	^{212}Bi(1^-)	415	5.363(38)	5.632	63.1(11)	46.3	26.6	0.0

[a] Δ_m is (expt. − theory)/expt. for $\overline{C(W)}^{1/2}$.

the inverse reaction ^{206}Pb$(n,p)^{206}$Tl. The distribution for $(M_0^T)^2$ will be, of course, nearly identical to that of $(M_0^S)^2$, i.e., see Eq. (29).

As expected, the spectra of Fig. 5 are dominated by a particle-hole "giant resonance." Since the placement of the Fermi surface is, as usual, arbitrary, it should be made clear that "particle-hole" in this context means a transition between a less than one-half-full shell and a more than one-half-full shell. The terms particle-particle and hole-hole have the same logic. As discussed in connection with core-polarization corrections (Sec. III C and Ref. 40) the large neutron excess and Pauli blocking limit the possible particle-hole terms contributing to the matrix elements to $\nu 0i_{11/2} \rightarrow \pi 0h_{11/2}$ for $R0$ and $\nu 0i_{11/2} \rightarrow \pi 0h_{11/2}$ and $\nu 1g_{9/2} \rightarrow \pi 0h_{11/2}$ for $R1$ in first order. Second-order transitions, i.e., those connecting np-nh admixtures in the initial state to mp-mh admixtures in the final state (transitions between the bottom two diagrams of Fig. 3) would not be discernable above the level of perception of Fig. 5 and thus this figure shows all the structure expected for this hypothetical experiment *no matter how much further the model space were enlarged.* Recall that other first-order effects have been incorporated via the $q_\alpha(j_i j_f)$ which, in this case, represent the effects of "particle-hole" admixtures in ^{206}Pb (see Fig. 3) and thus would be manifested by "giant resonances" in ^{206}Pb if the reverse experiment were performed.

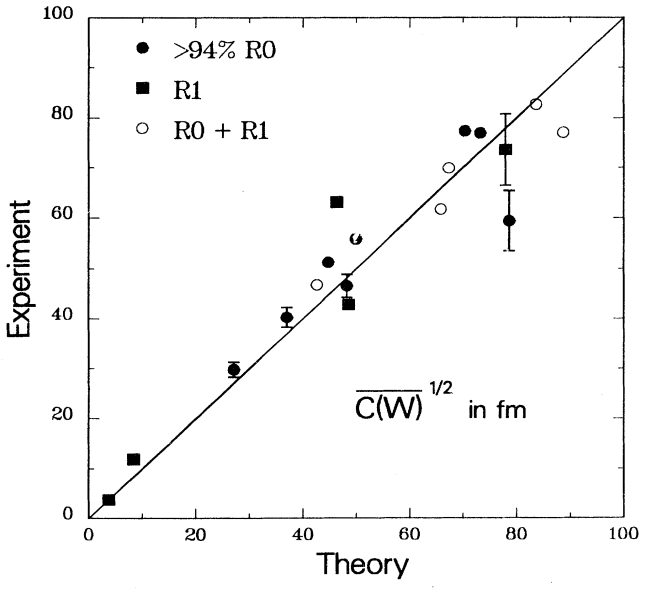

FIG. 4. Comparison of experimental and theoretical values of $\overline{C(W)}^{1/2}$ for the eighteen decays of Table V. Experimental uncertainties are shown only if they exceed the size of the symbols.

Let us consider $R0$ decays. The contributions to the ^{206}Hg(0^+) → ^{206}Tl 0_1^- decay shown in Table VI show a pronounced coherency. All single-particle transitions are in phase except the $\nu 0i_{11/2} \rightarrow \pi 0h_{11/2}$ particle-hole transition. This behavior is due to the general nature of the interaction; the particle-particle and hole-hole interactions are attractive so that — as explained by the schematic model [49] — the hole-hole plus particle-particle strength is concentrated in one (or a few) state and pushed to low energy in the same manner and to a

TABLE VI. Predicted values for the rank-zero $D_R(j_i j_f)$ and matrix elements of Eq. (1) for the decay of ^{206}Hg(0^+) to the first 0^- state of ^{206}Tl.

νj_i	πj_f	$D_0(j_i j_f)$	$M_0^S(j_i j_f,\text{eff})$	$\mathcal{M}_0^S(j_i j_f)$	$M_0^T(j_i j_f,\text{eff})$	$\mathcal{M}_0^T(j_i j_f)$
$1f_{7/2}$	$0g_{7/2}$	0.0021	−5.6855	−0.0119	165.8134	0.3465
$1f_{5/2}$	$1d_{5/2}$	−0.0184	14.5822	−0.2683	−217.1670	3.9959
$2p_{3/2}$	$1d_{3/2}$	0.0630	−8.2489	−0.5199	123.1460	7.7619
$2p_{1/2}$	$2s_{1/2}$	−0.8078	7.5419	−6.0926	−112.5725	90.9394
$0i_{11/2}$	$0h_{11/2}$	0.0613	22.0930	1.3552	−421.9811	−25.8843
$1g_{9/2}$	$0h_{9/2}$	0.0036	−8.9272	−0.0320	143.8030	0.5163
		Totals:		−5.5696		77.6757

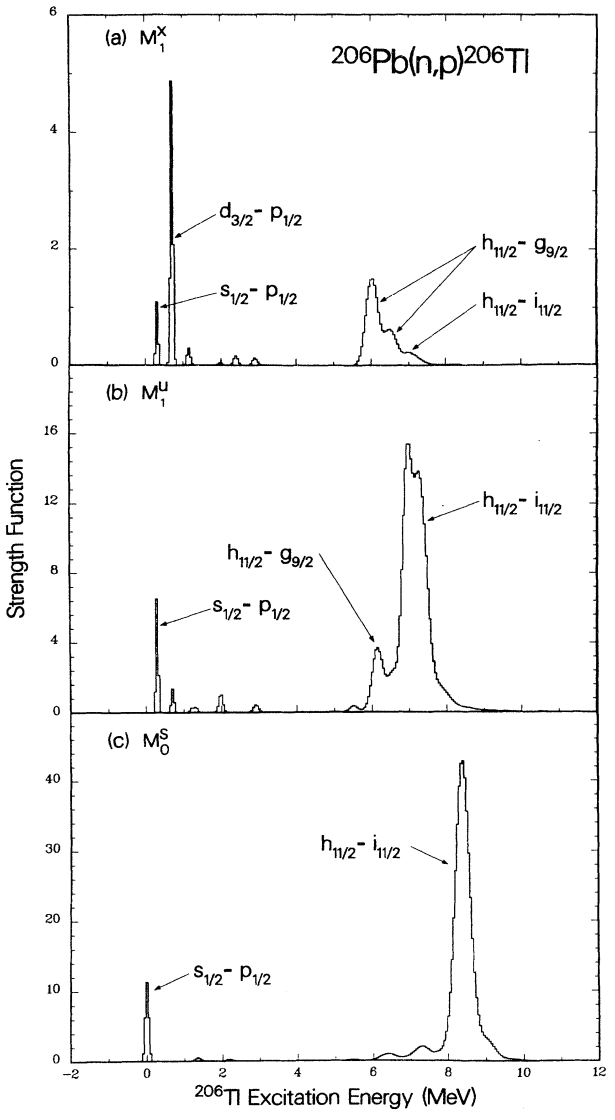

FIG. 5. Strength distributions (matrix-elements squared) for $R0$ and $R1$ matrix elements connecting excited states of ^{206}Tl to the 0^+ ground state of ^{206}Pb. The theoretical distributions have been folded with a Gaussian for ease of viewing and to simulate the experimental resolution which might pertain for the inverse charge-exchange reaction. The dominant $\nu - \pi$ transition is indicated for the major structures.

comparable degree as the familar 2_1^+ state in even-even nuclei. Likewise, the particle-hole interaction is repulsive so the particle-hole strength is concentrated at higher energies and the particle-hole contribution to lower states will be destructive. With two exceptions, this simple behavior is observed for all the $R0$ contributions of Table V. These exceptions are connected to the concept that the hole-hole plus particle-particle strength is isolated in a very few states — usually only one. Let us call this strength a "pygmy" resonance. It is expected that initial states will have a "pygmy" resonance in the final nucleus as well. The exception to the coherency occurs when the initial and final states are not each others "pygmy" resonances. Transitions between other states will, of course, not display this strong coherence, and, in fact, can be expected to display a great deal of destructive interference. In some instances we observe a state for which the destructive interference is maximal with all other terms except the dominant one in phase with each other and out of phase with the dominant term. We term this state "anticoherent." Again, initial states can have a (p,n) "anticoherent" state in the final nucleus just as well as final states have (n,p) "anticoherent" states in the initial nucleus.

For the decays of Table V there are two cases for which the "pygmy" resonance does not include the lowest-lying state. These are ^{208}Tl(5^+) $\rightarrow$ ^{208}Pb(5_1^-) and ^{211}Pb($\frac{9}{2}^+$) $\rightarrow$ ^{211}Bi($\frac{9}{2_1}^-$). In the first case, the (p,n) "pygmy" resonance of the ^{208}Tl(5_1^+) state is isolated in the ^{208}Pb 5_2^- state — in the $R0$ decay to the 5_1^- state all other single-particle contributions are destructive to $\nu 2p_{1/2} \rightarrow \pi 2s_{1/2}$ and so this is a classic "anti-coherent" state. Nevertheless, the $\nu 2p_{1/2} \rightarrow \pi 2s_{1/2}$ transition is dominant enough so that the branch to the 5_1^- state has a low $\log f_0 t$. In the $A = 211$ case, the decay to the $\frac{9}{2_1}^-$ state exhibits the same "anti-coherent" behavior, with the $\nu 1g_{9/2} \rightarrow \pi 0h_{9/2}$ transition dominant. The (p,n) "pygmy" resonance resides in the $\frac{9}{2_2}^-$ and $\frac{9}{2_3}^-$ states which share the strength found to reside in only the lowest state in most cases considered here.

The $R1$ decays can be understood in the same way, but the remarkable clarity of the effects observed for $R0$ decays is diminished by (a) the relaxation of the ΔJ rule from 0 to ≤ 1, and (b) the larger spread in the magnitude of $M_1^x(j_i j_f,\text{eff})$ as compared to $M_0^S(j_i j_f,\text{eff})$ and $M_1^u(j_i j_f,\text{eff})$ seen by comparing Tables VI and VII. In

TABLE VII. Predicted values for the rank-one $D_R(j_i j_f)$ and matrix elements of Eq. (1) for the decay of ^{206}Hg(0^+) to the first 1^- state of ^{206}Tl.

νj_i	πj_f	$D_1(j_i j_f)$	$M_1^u(j_i j_f,\text{eff})$	$\mathcal{M}_1^u(j_i j_f)$	$M_1^x(j_i j_f,\text{eff})$	$\mathcal{M}_1^x(j_i j_f)$
$0h_{9/2}$	$0g_{7/2}$	−0.0012	−7.0938	0.0089	7.6417	−0.0096
$1f_{7/2}$	$0g_{7/2}$	0.0005	−2.9945	−0.0014	−0.4032	−0.0002
$1f_{5/2}$	$0g_{7/2}$	0.0004	2.2938	0.0008	2.4710	0.0009
$1f_{7/2}$	$1d_{5/2}$	−0.0004	5.7366	−0.0025	6.1797	−0.0027
$1f_{5/2}$	$1d_{5/2}$	−0.0062	−7.9171	0.0490	1.2744	−0.0079
$2p_{3/2}$	$1d_{5/2}$	−0.0049	−3.2010	0.0158	3.4487	−0.0171
$1f_{5/2}$	$1d_{3/2}$	−0.0585	−3.4826	0.2038	4.6400	−0.2715
$2p_{3/2}$	$1d_{3/2}$	0.0206	−3.9660	−0.0818	−1.2445	−0.0257
$2p_{1/2}$	$1d_{3/2}$	0.0583	2.6324	0.1535	2.6867	0.1567
$2p_{3/2}$	$2s_{1/2}$	0.1224	2.7530	0.3370	3.2577	0.3987
$2p_{1/2}$	$2s_{1/2}$	−0.7810	−4.4675	3.4889	2.4062	−1.8792
$0i_{13/2}$	$0h_{11/2}$	−0.0021	19.4398	−0.0404	15.4223	−0.0321
$0i_{11/2}$	$0h_{11/2}$	0.0354	−15.7455	−0.5569	1.0307	0.0365
$1g_{9/2}$	$0h_{11/2}$	0.0286	−4.4843	−0.1284	4.2213	0.1209
$0i_{11/2}$	$0h_{9/2}$	−0.0019	−5.3612	0.0099	8.1391	−0.0151
$1g_{9/2}$	$0h_{9/2}$	−0.0027	−3.3391	0.0090	−0.5600	0.0015
$1g_{9/2}$	$1f_{7/2}$	0.0004	5.1674	0.0022	6.7910	0.0029
$0j_{15/2}$	$0i_{13/2}$	0.0000	9.1293	0.0000	11.3392	0.0000
		Totals:		3.4673		−1.5427

Fig. 5 the effect of (a) is seen to spread the "giant" and "pygmy" resonances although they are still concentrated at high and low energy respectively. A noticeable effect of (b) is the diminished strength of the $\nu 0i_{11/2} \rightarrow \pi 0h_{11/2}$ $(M_1^x)^2$ strength due to the unusually small value of $M_1^x(j_i j_f,\text{eff})$ for this transition. In spite of these diminishing effects, the decay shown in Table VII exhibits similar coherency to the $R0$ decay of Table VI. For instance, the M_1^u matrix element of Table VII can be decomposed into a "hole-hole + particle-particle" contribution and a "particle-hole" contribution: 3.4673 = 4.1526 − 0.6853 fm^2. The collectivity manifest in the "pygmy" resonance is such that the out-of-phase contribution to the first term on the right is only 2%. The behavior of the $M_1^u(j_i j_f,\text{eff})$ and $M_1^x(j_i j_f,\text{eff})$ matrix elements for the other $R1$ contributions of Table V follows quite closely to that described for the $R0$ matrix elements, including the abnormal behavior for ^{208}Tl and ^{211}Pb decay.

The major distinction between the $R0$ and $R1$ decays is in how the matrix elements combine to form the total $B_1^{(R)}$. The simple relationship between the two $R0$ matrix elements [Eqs. (29) and (30)] is such that in β^- decay in the lead region the two matrix elements will always add destructively. In contrast, the relative sign of $M_1^u(j_i j_f,\text{eff})$ and $M_1^x(j_i j_f,\text{eff})$ depends on j_i and j_f and, as was noted in the discussion of Eq. (27), the strength of $R1$ decays depends critically on this relative sign. This phase is constructive for $\nu 2p_{1/2} \rightarrow \pi 2s_{1/2}$ transitions with the result that the $R1$ contributions to the first nine listed transitions of Table V have constructive contributions from M_1^u and M_1^x and are strong. The dominant $R1$ contribution to all the remaining decays of Table V except the last is $\nu 1g_{9/2} \rightarrow \pi 0h_{9/2}$. As shown in Table VIII, the contributions of $M_1^u(j_i j_f,\text{eff})$ and $M_1^x(j_i j_f,\text{eff})$ are destructive for this transition and, in addition, the magnitude of $M_1^x(j_i j_f,\text{eff})$ is very small. These conditions result in relatively weak decay rates. Thus, the decays listed in Table V for ^{209}Pb and ^{211}Pb are almost pure $R0$ decays and the decays of ^{210,212,214}Pb to the 1^- ground states of ^{210,212,214}Bi shown in Fig. 1 all have large $\log f_0 t$ values.

The one strong $R1$ decay not considered is ^{212}Pb(0^+) $\rightarrow$ ^{212}Bi(1_2^-) listed last in Table V and detailed in Table VIII. The largest contributions to the matrix elements are $\nu 0i_{11/2} \rightarrow \pi 0h_{9/2}$ and $\nu 1g_{9/2} \rightarrow \pi 1f_{7/2}$ which add destructively for M_1^u and constructively for M_1^x. The result is that the transition is dominated by M_1^x and is relatively strong.

The three ^{214}Pb $\rightarrow$ ^{214}Bi decays shown in Fig. 1 show strong similarities to the three ^{212}Pb $\rightarrow$ ^{212}Bi decays. This similarity was discussed in terms of a generalized seniority scheme in a recent study of ^{214}Pb $\rightarrow$ ^{214}Bi [50].

The three decays of Table V for which theory disagrees with experiment by more than 15% merit some discussion. One of these, the decay to the 1^- ground state of ^{212}Bi has a very large $\log f_0 t$ value which results from the strong cancellation between M_1^u and M_1^x discussed above. Essentially insignificant (from any other point-of-view) changes in the wave functions would be necessary in order to reproduce experiment and there is the possibility of higher-order Coulomb effects (see Ref. 43) so that this disagreement is not serious. It is likely that the disagreement for the decay to the 1_2^- state of ^{212}Bi is due to inadequacies in its wave function. The basis states which are dominant in the 1_2^- and 1_3^- states, respectively, have closely equal unperturbed energies and are predicted to mix rather strongly with the consequence that the $\log f_0 t$ values for the branches to these two states are considerably more sensitive to the interaction than the other decays of Table V. The most serious disagreement is for the ^{206}Hg(0^+) $\rightarrow$ ^{206}Tl(0^-) branch. Actually the large experimental uncertainty for this branch results from an

uncertainty in how the decay is divided between the 0_1^- and 1_1^- states of ^{206}Tl. The prediction for the average of the two $\overline{C(W)}^{1/2}$ is 19% too large. This is probably due to a deficiency in the wave functions and that for the ^{206}Hg 0_1^+ wave function seems most likely at fault. Very little experimental information is available for the ^{206}Hg energy levels [51], and the adjustment made by Rydström, *et al.* [28] in the KHH *pp* interaction in order to obtain the KHH$_e$ interaction is more arbitrary than for the *nn* or *pn* parts of the interaction. We note that in the KHH$_e$ interaction the ^{206}Pb ground state is 51% $\nu 2p_{1/2}^{-2}$ while the ^{206}Hg ground state is 71% $\pi 2s_{1/2}^{-2}$. A decrease in the latter would result in improved agreement with experiment.

We now turn to a discussion of further decays in $A = 205$–211 nuclei and to neutrino capture by ^{205}Tl. In the remainder of this article all transitions are calculated with $\epsilon_{\rm mec} = 2.0$, and $sq_1 = sq_x = sq_u = 1.0$ unless otherwise specified.

V. SOME ADDITIONAL DECAYS

A. ^{205}Hg(β^-)^{205}Tl

In addition to the ^{205}Hg($\frac{1}{2}_1^-$) $\rightarrow$ ^{205}Tl($\frac{1}{2}_1^+$) decay, ^{205}Hg decays to two further $\frac{1}{2}^+$ states, three $\frac{3}{2}^+$ states and the 619-keV $\frac{5}{2}^+$ state in ^{205}Tl. The decays to the $\frac{1}{2}^+$

TABLE VIII. Predicted values for the rank-one $D_R(j_i j_f)$ and matrix elements of Eq. (1) for the decay of ^{212}Pb(0^+) to the first two 1^- states of ^{212}Bi.

νj_i	πj_f	$D_1(j_i j_f)$	$M_1^u(j_i j_f,\text{eff})$	$\mathcal{M}_1^u(j_i j_f)$	$M_1^x(j_i j_f,\text{eff})$	$\mathcal{M}_1^x(j_i j_f)$
			^{212}Bi $J_k^\pi = 1_1^-$			
$0i_{11/2}$	$0h_{11/2}$	0.0092	−15.3354	−0.1406	0.8581	0.0079
$1g_{9/2}$	$0h_{11/2}$	−0.0003	−4.1577	0.0015	3.8934	−0.0014
$0i_{11/2}$	$0h_{9/2}$	0.0019	−4.3571	−0.0084	7.6299	0.0147
$1g_{9/2}$	$0h_{9/2}$	−0.4702	−3.5705	1.6790	−0.5139	0.2417
$1g_{7/2}$	$0h_{9/2}$	0.0179	3.1110	0.0557	2.7802	0.0497
$1g_{9/2}$	$1f_{7/2}$	0.0037	4.7712	0.0175	6.7240	0.0247
$1g_{7/2}$	$1f_{7/2}$	0.0025	−9.4245	−0.0233	0.8799	0.0022
$2d_{5/2}$	$1f_{7/2}$	−0.0009	−3.2398	0.0030	3.4943	−0.0032
$1g_{7/2}$	$1f_{5/2}$	0.0001	−3.7021	−0.0003	5.6452	0.0005
$2d_{5/2}$	$1f_{5/2}$	−0.0038	−5.3554	0.0204	−1.1416	0.0043
$2d_{3/2}$	$1f_{5/2}$	0.0012	3.6372	0.0043	3.7133	0.0043
$2d_{5/2}$	$2p_{3/2}$	0.0007	4.6373	0.0032	5.5393	0.0038
$2d_{3/2}$	$2p_{3/2}$	0.0003	−6.7930	−0.0017	1.6496	0.0004
$3s_{1/2}$	$2p_{3/2}$	0.0000	−3.0435	0.0001	3.5264	−0.0001
$2d_{3/2}$	$2p_{1/2}$	0.0000	−2.8672	−0.0001	3.7316	0.0002
$3s_{1/2}$	$2p_{1/2}$	−0.0006	−4.3932	0.0026	−2.6384	0.0016
$0j_{15/2}$	$0i_{13/2}$	0.0074	9.0837	0.0674	11.5820	0.0859
		Totals:		1.6799		0.4373
			^{212}Bi $J_k^\pi = 1_2^-$			
$0i_{11/2}$	$0h_{11/2}$	−0.0008	−15.3354	0.0126	0.8581	−0.0007
$1g_{9/2}$	$0h_{11/2}$	0.0100	−4.1577	−0.0416	3.8934	0.0390
$0i_{11/2}$	$0h_{9/2}$	−0.1594	−4.3571	0.6944	7.6299	−1.2160
$1g_{9/2}$	$0h_{9/2}$	0.0535	−3.5705	−0.1910	−0.5139	−0.0275
$1g_{7/2}$	$0h_{9/2}$	−0.0080	3.1110	−0.0247	2.7802	−0.0221
$1g_{9/2}$	$1f_{7/2}$	−0.1110	4.7712	−0.5297	6.7240	−0.7464
$1g_{7/2}$	$1f_{7/2}$	−0.0009	−9.4245	0.0088	0.8799	−0.0008
$2d_{5/2}$	$1f_{7/2}$	−0.0026	−3.2398	0.0086	3.4943	−0.0092
$1g_{7/2}$	$1f_{5/2}$	−0.0066	−3.7021	0.0242	5.6452	−0.0370
$2d_{5/2}$	$1f_{5/2}$	0.0016	−5.3554	−0.0085	−1.1416	−0.0018
$2d_{3/2}$	$1f_{5/2}$	−0.0012	3.6372	−0.0043	3.7133	−0.0044
$2d_{5/2}$	$2p_{3/2}$	−0.0024	4.6373	−0.0113	5.5393	−0.0135
$2d_{3/2}$	$2p_{3/2}$	−0.0004	−6.7930	0.0025	1.6496	−0.0006
$3s_{1/2}$	$2p_{3/2}$	−0.0007	−3.0435	0.0020	3.5264	−0.0023
$2d_{3/2}$	$2p_{1/2}$	−0.0011	−2.8672	0.0031	3.7316	−0.0041
$3s_{1/2}$	$2p_{1/2}$	0.0010	−4.3932	−0.0043	−2.6384	−0.0026
$0j_{15/2}$	$0i_{13/2}$	−0.0198	9.0837	−0.1796	11.5820	−0.2290
		Totals:		−0.2388		−2.2789

and $\frac{3}{2}^+$ states were considered with the PKH interaction alone. The results are compared to experiment in Table IX. For the results of Table V the KHH$_e$ interaction produced the main part of the $D_R(j_i j_f)$ for $A = 205$ with input for the $j = \frac{9}{2}$ and $\frac{11}{2}$ orbits from the PKH interaction. A comparison of the results for the ^{205}Tl ground state given in Tables V and IX reveals quite good agreement between the KHH$_e$ and PKH interactions.

The agreement with experiment for the decays of Table IX is satisfactory. For both the $\frac{1}{2}^+$ and $\frac{3}{2}^+$ states the experimental $\log f_0 t$ values have a small-large-small pattern with increasing E_x (or k). This is well produced by the PKH interaction. The decays to the $\frac{1}{2}^+$ states are all found to involve comparable contributions from both $R0$ and $R1$. The decays to the $\frac{3}{2}^+$ states are $R1$ with, as expected, insignificant contributions from $R2$. Both the $R0$ and $R1$ components of the three $\frac{1}{2}^+$ decays are predominantly $\nu 2p_{1/2} \rightarrow \pi 2s_{1/2}$ for which M_1^x and M_1^u contribute constructively to the $R1$ rate. The individual contributions of the $M_R^\alpha(j_i j_f)$ to the $R0$ and $R1$ rates have the same general behavior as k increases: the $k = 1$ state is the "pygmy" resonance and $k = 3$ is the "anticoherent" state with some leakover into $k = 2$.

For all three $\frac{3}{2}^+$ states $\nu 2p_{3/2} \rightarrow \pi 2s_{1/2}$ is dominant. For these transitions the M_1^x and M_1^u contributions are out of phase so that these decays are inherently weaker than those to the $\frac{1}{2}^+$ states. The (n,p) "pygmy" resonance for both M_1^u and M_1^x is divided between the $k = 1$ and $k = 3$ states whose decays, therefore, have strong, rather coherent contributions from the individual single-particle transitions. The M_1^u and M_1^x are nearly equal so that the decay rates are determined by the latter [see Eq. (31)]. The $k = 2$ decay has small values of M_1^x and M_1^u whose contributions nearly cancel.

The $R2$ decay to the $\frac{5}{2_1}^+$ state is the first unique first-forbidden decay we have considered. The experimental and KHH (+PKH) values for the beta-moment, $B_1^{(2)}$, are 5.3 ± 2.1 and 4.89 fm^2, respectively. The decay is found to be largely $\nu 2p_{3/2} \rightarrow \pi 2s_{1/2}$ with significant $\nu 2p_{1/2} \rightarrow \pi 1d_{5/2}$ and $\nu 1f_{7/2} \rightarrow \pi 1d_{3/2}$ contributions. It is highly coherent with only 2% out-of-phase contribution, i.e., it also has the characteristics of a "pygmy" resonance. Thus it is relatively insensitive to variations in the wave functions so that the good agreement with experiment is encouraging.

TABLE IX. β^- branching ratios (BR) and $\log f_0 t$ values for the decay of ^{205}Hg to low-lying states of ^{205}Tl. The index k orders the ^{205}Tl levels of a given J^π in energy.

		Experiment		Theory (PKH)	
J_k^π	E_x(keV)	BR(%)	$\log f_0 t$	BR(%)	$\log f_0 t$
$\frac{1}{2_1}^+$	0.0	96.8(15)	5.274(12)	85.4	5.33
$\frac{1}{2_2}^+$	1219.2	0.007(4)	$7.05^{+0.38}_{-0.24}$	0.0074	7.02
$\frac{1}{2_3}^+$	1434.5	0.005(3)	$5.64^{+0.40}_{-0.23}$	0.0019	6.03
$\frac{3}{2_1}^+$	203.7	3.2(13)	$6.53^{+0.23}_{-0.15}$	2.45	6.64
$\frac{3}{2_2}^+$	1140.7	0.004(2)	$7.64^{+0.30}_{-0.18}$	0.0078	7.32
$\frac{3}{2_3}^+$	1340.3	0.006(3)	$6.45^{+0.30}_{-0.18}$	0.0043	6.59
$\frac{5}{2_1}^+$	619.4	0.015(7)	$8.27^{+0.30}_{-0.18}$	0.0065	8.63

B. ^{205}Pb($\frac{5}{2}^-$) $\rightarrow$ ^{205}Tl($\frac{1}{2}^+$) EC decay

The extraction of the experimental value for the beta-moment of this electron capture transition is described in Appendix D. The result is $B_1^{(2)} = (5.0 \pm 0.6) \times 10^{-3}$ fm^2. Comparing to the value $B_1^{(2)} = (5.3 \pm 2.1)$ fm^2 for the ^{205}Hg($\frac{1}{2}^+$) $\rightarrow$ ^{205}Tl($\frac{5}{2}^-$) decay just described, we see that this EC decay is highly forbidden. In fact from the theoretical point of view the beta-moment is essentially zero. The KHH$_e$ prediction for this decay was made with a large-scale calculation with dimensions of 3092 and 2538 for the initial $\frac{5}{2}^-$ and final $\frac{1}{2}^+$ states, respectively. The ^{205}Pb $\frac{5}{2}^-$ ground state is found to be largely $\nu 1f_{5/2}^{-1} 2p_{1/2}^{-2}$ (65%) and $\nu 1f_{5/2}^{-1} 2p_{3/2}^{-2}$ (15%) while the ^{205}Tl $\frac{1}{2}^+$ ground state is largely $\pi 2s_{1/2}^{-1} \nu 2p_{1/2}^{-2}$ (43%), $\pi 2s_{1/2}^{-1} \nu 2p_{3/2}^{-2}$ (15%), and $\pi 2s_{1/2}^{-1} \nu 1f_{5/2}^{-2}$ (16%). The $D_R(j_i j_f)$ for the $\nu 1f_{5/2} \rightarrow \pi 2s_{1/2}$ transition is overwhelmingly dominant but is Δl forbidden and so only proceeds via the core-polarization effect (see Sec. V E). The result is that the decay is composed of incoherent contributions from small components which nearly cancel. For instance, if a constant quenching factor is used, rather than different $q_z(j_i j_f)$ for each $j_i \rightarrow j_f$ transition, the sign of M_2^z is reversed. In view of this, the PKH result of $B_1^{(2)} = 22 \times 10^{-3}$ is considered to be in excellent agreement with experiment.

C. Neutrino capture by ^{205}Tl

1. *Formalism*

We are interested in the neutrino capture process

$$\nu_e + (Z, A) \rightarrow (Z + 1, A) + e^-, \tag{34}$$

which is energetically possible for $W_\nu > \Delta$ where [52]

$$\Delta = [M(Z + 1, A) - M(Z, A)] + \overline{E}_{\rm ex}. \tag{35}$$

In Eq. (35), the term in brackets is the atomic mass difference, $\overline{E}_{\rm ex}$ is the average excitation energy of the final atom, and, as usual, all energies are in natural units unless otherwise specified. For $\overline{E}_{\rm ex}$ we use the approximation, due to Bahcall [52], of $23Z^{2/5}$ eV when $Z > 10$. The energy of the continuum electron is

$$W_e = W_\nu - \Delta + 1, \tag{36}$$

where we follow the previous custom of designating the electron energy W as W_e when discussing neutrino capture. For small enough values of W_ν and W_e where the long-wavelength approximation applies, i.e., $p_\nu R << 1, p_e R << 1, W_e R << 1$, and the condition $(W_\nu + W_e)R < 1$ is fulfilled, neutrino capture bears a simple and exact relation to the analogous β^- decay process.

In the Behrens-Bühring formalism [19] the cross section for neutrino capture in the long-wavelength limit is

$$\sigma = 2.629 \times 10^{-41} S p_e W_e F(Z, W_e) \frac{C(W_e)_\nu}{6166 \lambda_{Ce}{}^{2n}} \text{ cm}^2, \tag{37}$$

where $S = (2J_f + 1)/(2J_i + 1)$, $F(Z, W_e)$ is the Fermi function and $C(W_e)_\nu$ is the β^- decay shape factor $C(W_e)$ in fm^2 but with $p_\nu \rightarrow -p_\nu$. In the Behrens-Bühring treatment p_ν does not directly enter up through first order, and since the first-order expansion should be adequate, we can use the normal β^- shape factor $C(W_e)$ for $C(W_e)_\nu$.

Equation (37) is valid for all degrees of forbiddeness. For allowed transitions ($n = 0$) calculated to first order, $C(W_e)$ is a constant and $6166/C(W_e)$ is the $f_0 t$ value of the analogous β^- decay in sec. Since the capture cross section is inversely proportional to it, the $f_0 t$ value provides a convenient and familiar measure of the dependence of the cross section on the nuclear structure of the initial and final states.

Recall that for first-forbidden transitions the β^- shape factor is

$$C(W_e) = k(1 + aW_e + b/W_e + cW_e^2). \tag{38}$$

In conventional β^- decay, k, ka, kb, kc are all functions of the end-point energy W_0. In the present application they are to be used with $W_0 = W_e + W_\nu = 2W_e + \Delta - 1$ so they are no longer independent of W_e. As in β decay, the shape factor contains all the information on the underlying nuclear structure. For forbidden neutrino capture $6166\lambda_{Ce}^2/C(W_e)$ can be thought of as an "effective" $f_0 t$ value but it is energy dependent and so this is not a rigorous analogy and, as we will see, the energy dependence must be taken into account in any quantitative calculation of neutrino-capture cross sections.

2. *Results at threshold*

From a recent determination of the ^{205}Pb–^{205}Tl atomic mass difference of 51.3(6) keV [53], $E_x = 2.3$ keV for the $\frac{1}{2}^-_1$ state of ^{205}Pb, and Eq. (35) we have $\Delta = 53.7(6)$ keV for the $\frac{1}{2}^-_1$ state; while, in general, $\Delta(J_k^\pi) = 51.4 + E_x(J_k^\pi)$ keV. Matrix elements were calculated for each of the first ten ^{205}Pb $\frac{1}{2}^-$ and $\frac{3}{2}^-$ states. These were then used to calculate the shape factor and effective $\log f_0 t$ value at threshold [$W_e = 1$, $W_0(J_k^\pi) = 1 + \Delta(J_k^\pi)$]. The results are given in Table X.

One important feature of the ν_e + ^{205}Tl reaction is the low threshold which renders it potentially sensitive to solar pp neutrinos [54]. Thus the important state in Table X is the $\frac{1}{2}^-_1$ state which also has the largest cross section at threshold. How reliable is the shape factor calculation for this state? To help answer this question, the contributions of the single-particle transitions to the total matrix elements are shown in Tables XI and XII. It is clear that that this transition is in the "anticoherent" class discussed in the last section. The (n, p) "pygmy" resonance for the ^{205}Pb($\frac{1}{2}^-_1$) state is found to be the $\frac{1}{2}^+_3$ state of ^{205}Tl which experimentally is at 1434 keV. The hypothetical $\log f_0 t_{W_e=1}$ value for ^{205}Tl($\frac{1}{2}^+_3$) $\rightarrow$ ^{205}Pb($\frac{1}{2}^-_1$) is predicted to be 5.210. From the large $\log f_0 t_{W_e=1}$ values for the capture into $\frac{1}{2}^-$ states of ^{205}Pb shown in Table X, it is clear that the $\frac{1}{2}^+_1$ state of ^{205}Tl does not have a pronounced low-lying $\frac{1}{2}^-$ (p, n) "pygmy" resonance in ^{205}Pb. This lack is made plausible from the fact that the dominant configuration of ^{205}Tl($\frac{1}{2}^+_1$) — $(\pi 2s_{1/2})^{-1}(\nu 2p_{1/2})^{-2}$ — cannot connect to $\frac{1}{2}^-$ states of ^{205}Pb by a particle-particle or hole-hole transition.

Closely related to this latter point, it has been asserted [55, 56, 28] that this transition will be retarded because the zeroth-order wave functions for the initial and final states are

$$|^{206}\text{Tl}\rangle = (\pi 2s_{1/2})^{-1}(\nu 2p_{1/2})^{-2},$$
$$|^{206}\text{Pb}\rangle = (\nu 2p_{1/2})^{-1}(\nu 2p_{3/2}, 1f_{5/2})^{-2}.$$

We find that this by itself is not a pertinent argument; for instance, the ^{205}Hg($\frac{1}{2}^-$) $\rightarrow$ ^{205}Tl($\frac{1}{2}^+$) transition of Table V has the low $\log f_0 t$ value of 5.274 and yet for this transition we find $D_R(\frac{1}{2}\frac{1}{2}) = 0.46$ for both $R0$ and $R1$ as opposed to $D_R(\frac{1}{2}\frac{1}{2}) = 0.60$ for the ^{205}Tl($\frac{1}{2}^+$) $\rightarrow$ ^{205}Pb($\frac{1}{2}^-$) transition. Rather, the important difference between the two decays is that ^{205}Hg($\frac{1}{2}^-$) $\rightarrow$ ^{205}Tl($\frac{1}{2}^+$) displays the classic coherency of a pygmy resonance while ^{205}Tl($\frac{1}{2}^+$) $\rightarrow$ ^{205}Pb($\frac{1}{2}^-$), shown in Tables XI and XII, is a classic anticoherent transition. To illustrate, if the magnitudes of all the $D_R(j_i j_f)$ for this latter transition were left unchanged but the signs were changed so as to produce a pygmy resonance, then the calculation would give $\log f_0 t_{W_e=1} = 5.116$.

Because of the anticoherency of this transition, it is considerably more sensitive to the wave functions than the faster decays of Table V. To illustrate this sensitivity, the same large-basis calculation was repeated with the SDI interaction. The main difference between the SDI and KHH$_e$ (+ PKH) results was in the $D_R(j_i j_f)$ which was 0.46 for the SDI interaction for both R0 and R1 as opposed to the magnitude of 0.60 of Tables XI and XII. The same complete anticoherence was found as shown in Tables XI and XII; the smaller value of $D_R(j_i j_f)$ results in increased cancellation and the final result of the SDI calculation is $\overline{C(W)}^{1/2}_{W_e=1} = 219$ fm^2, $\log f_0 t_{W_e=1} = 6.62$. In conclusion, the calculation of the decay parameters for ^{205}Tl($\frac{1}{2}^+$) $\rightarrow$ ^{205}Pb($\frac{1}{2}^-$) is considerably less reliable than for the fast decays of Table V.

3. *The effect of increasing neutrino energy*

If the incident neutrino energy rises significantly above threshold then there is a further complexity and source of uncertainty in the calculation of the total capture cross section. This uncertainty is connected to the energy dependence of the $C(W_e)$ value. At threshold, i.e., $W_e - 1$

TABLE X. Predictions for matrix elements, shape factors and effective $\log f_0 t$ values for neutrino capture by ^{205}Tl leading to the lowest ten $\frac{1}{2}^-$ and $\frac{3}{2}^-$ states of ^{205}Pb. Both $C(W_e)$ and $\log f_0 t$ were evaluated at threshold, i.e., for $W_e = 1$.

J^π	k	Rank	M_0^S/M_1^u	M_0^T/M_1^x	C(W_e)	$\log f_0 t$
$\frac{1}{2}^-$	1	0	−1.863	50.50		
		1	1.426	−0.495	1504.8	5.786
	2	0	−0.308	9.47		
		1	0.197	−0.344	156.8	6.768
	3	0	−0.562	16.28		
		1	0.480	−0.226	187.1	6.69
	4	0	−0.299	9.04		
		1	0.090	−0.047	27.0	7.54
	5	0	−0.524	15.86		
		1	0.380	−0.131	127.0	6.86
	6	0	−0.131	3.98		
		1	0.018	0.018	4.0	8.35
	7	0	−0.151	4.56		
		1	0.041	0.054	6.0	8.20
	8	0	−0.298	9.03		
		1	0.304	−0.193	90.0	7.01
	9	0	−0.029	0.89		
		1	0.056	−0.052	5.0	8.31
	10	0	−0.129	3.90		
		1	0.064	−0.008	4.0	8.46
$\frac{3}{2}^-$	1	1	1.424	1.754	480.2	6.282
	2	1	0.408	−0.055	35.1	7.419
	3	1	0.335	0.250	3.2	8.46
	4	1	0.159	0.282	27.0	7.53
	5	1	0.023	0.046	1.0	9.10
	6	1	0.192	−0.083	18.0	7.72
	7	1	0.089	0.180	13.0	7.84
	8	1	0.169	0.155	5.0	8.30
	9	1	0.110	0.097	1.0	9.08
	10	1	0.006	0.057	2.0	8.66

[a] For the evaluation of C(W_e) as a function of incident neutrino energy the parameters r'_w, r'_u, and r'_x of Sec III D 1 are also needed. These are approximately state independent. The three values for the $\frac{1}{2}^-_1$ state are all equal to 0.81.

$= 0.0$, the shape factor for the $\frac{1}{2}^-$ state is calculated to be [57]

$$C(W_e) = 1438.6 + 54.8W_e + 10.2/W_e + 1.24W_e^2 = 1505 \text{ fm}^2 \quad (W_e = 1). \tag{39}$$

which, using Eq. (24), gives a $\log f_0 t_{W_e=1}$ value of 5.786. At a neutrino energy of $9 + \Delta = 4.7$ MeV such that $W_e = 10$, the shape factor becomes

$$C(W_e) = 787.8 + 41.85W_e + 3.1/W_e + 1.05W_e^2 = 1312 \text{ fm}^2 \quad (W_e = 10). \tag{40}$$

The explicit dependence on W_e increases markedly with energy but when the energy dependence (via W_0) of k, ka, kb, kc are taken into account the shape factor is changed very little. It has decreased from its threshold value by 2.5% at $W_e = 2$ and 7.5% at $W_e = 10$ and is

TABLE XI. Predicted values for the rank-zero $D_R(j_i j_f)$ and matrix elements of Eq. (1) for the neutrino capture by ^{205}Tl($\frac{1}{2}^+$) leading to the lowest $\frac{1}{2}^-$ state of ^{205}Pb.

νj_i	πj_f	$D_0(j_i j_f)$	$M_0^S(j_i j_f,\text{eff})$	$\mathcal{M}_0^S(j_i j_f)$	$M_0^T(j_i j_f,\text{eff})$	$\mathcal{M}_0^T(j_i j_f)$
$1f_{7/2}$	$0g_{7/2}$	0.0042	4.0235	0.0168	−117.2423	−0.4889
$1f_{5/2}$	$1d_{5/2}$	−0.0622	−10.0806	0.6272	158.0203	−9.8314
$2p_{3/2}$	$1d_{3/2}$	0.0614	5.7910	0.3557	−87.5424	−5.3774
$2p_{1/2}$	$2s_{1/2}$	0.6031	−5.3560	−3.2303	79.5947	48.0051
$0i_{11/2}$	$0h_{11/2}$	−0.0235	−15.5370	0.3649	298.8035	−7.0175
$1g_{9/2}$	$0h_{9/2}$	0.0004	6.4366	0.0024	−101.3038	−0.0374
		Totals:		−1.8633		25.2526

TABLE XII. Predicted values for the rank-one $D_R(j_i j_f)$ and matrix elements of Eq. (1) for the neutrino capture by ^{205}Tl($\frac{1}{2}^+$) leading to the lowest $\frac{1}{2}^-$ state of ^{205}Pb.

νj_i	πj_f	$D_1(j_i j_f)$	$M_1^u(j_i j_f,\text{eff})$	$\mathcal{M}_1^u(j_i j_f)$	$M_1^x(j_i j_f,\text{eff})$	$\mathcal{M}_1^x(j_i j_f)$
$0h_{9/2}$	$0g_{7/2}$	0.0024	−5.0111	−0.0122	5.3981	0.0131
$1f_{7/2}$	$0g_{7/2}$	−0.0015	−2.1191	0.0033	−0.2853	0.0004
$1f_{5/2}$	$0g_{7/2}$	0.0035	1.6399	0.0057	1.7666	0.0061
$1f_{7/2}$	$1d_{5/2}$	0.0035	4.0426	0.0143	4.3549	0.0154
$1f_{5/2}$	$1d_{5/2}$	0.0210	−5.5819	−0.1173	0.8985	0.0189
$2p_{3/2}$	$1d_{5/2}$	0.0139	−2.2593	−0.0314	2.4341	0.0338
$1f_{5/2}$	$1d_{3/2}$	0.0973	−2.4555	−0.2389	3.2715	0.3182
$2p_{3/2}$	$1d_{3/2}$	−0.0114	−2.7993	0.0319	−0.8784	0.0100
$2p_{1/2}$	$1d_{3/2}$	0.0000	1.8587	0.0001	1.8970	0.0001
$2p_{3/2}$	$2s_{1/2}$	−0.0072	1.9417	−0.0140	2.2977	−0.0166
$2p_{1/2}$	$2s_{1/2}$	−0.6025	−3.1515	1.8988	1.6975	−1.0227
$0i_{13/2}$	$0h_{11/2}$	0.0067	13.7106	0.0918	10.8771	0.0728
$0i_{11/2}$	$0h_{11/2}$	0.0145	−11.1041	−0.1606	0.7269	0.0105
$1g_{9/2}$	$0h_{11/2}$	0.0140	−3.1649	−0.0443	2.9792	0.0417
$0i_{11/2}$	$0h_{9/2}$	0.0004	−3.7811	−0.0016	5.7401	0.0024
$1g_{9/2}$	$0h_{9/2}$	0.0003	−2.3564	−0.0008	−0.3952	−0.0001
$1g_{9/2}$	$1f_{7/2}$	0.0002	3.6447	0.0009	4.7898	0.0012
$0j_{15/2}$	$0i_{13/2}$	0.0000	6.4432	0.0000	8.0029	0.0000
		Totals:		1.4258		−0.4948

slowly varying from threshold to the latter point. That this slow variation of $C(W_e)$ with neutrino energy is accidental is shown by a consideration of the shape factor for the $\frac{3}{2}^-_1$ state of ^{205}Pb at E_x = 263 keV for which Δ = 825.3 keV. For it we find

$$C(W_e) = 489.2 - 48.7W_e + 37.2/W_e + 2.49W_e^2 = 480 \text{ fm}^2 \quad (W_e = 1) \tag{41}$$

with an $\log f_0 t_{W_e=1}$ value = 6.282. At W_ν = 4.91 MeV (W_e = 10) the shape factor becomes

$$C(W_e) = 3227.3 - 153.5W_e + 87.4/W_e + 2.49W_e^2 = 1980 \text{ fm}^2 \quad (W_e = 10) \tag{42}$$

leading to an effective $\log f_0 t$ of 5.666. Thus at W_ν = 4.91 MeV the cross section for capture into the $\frac{3}{2}^-_1$ state is calculated to be ~4 times larger than would be predicted from $C(W_e = 1)$ assuming an energy-independent shape factor.

D. ^{206}Hg(β^-)^{206}Tl

In addition to the 0^-_1 and 1^-_1 states of ^{206}Tl, ^{206}Hg has a branch of (3 ± 2)% into the 1^-_2 state at 649 keV in ^{206}Tl [51]. The KHH$_e$ (+KPH) calculation for this branch gives 1.9% from $\log f_0 t$ = 5.87 in agreement with experiment. No other β^- branches are known. We predict $\log f_0 t$ = 5.88 for the third 1^- level. If it is at 940 keV (its lowest likely placement) its predicted branch is 0.27%. These decays illustrate that the (n,p) pygmy resonances for M_1^u and M_1^x are more diffuse than encountered for $R0$ decays. For instance, that for M_1^x is spread over the k = 2–4 1^- levels of ^{206}Tl. The 0^-_2 state is not known experimentally. With the KHH$_e$ interaction it is predicted at E_x = 1361 keV and is therefore not accessible for β^- decay.

E. ^{206}Tl(β^-)^{206}Pb

Branches of 0.055(5)% and 0.09(2)% to the 2^+_1 and 0^+_2 states of ^{206}Pb are known in ^{206}Tl β^- decay as well as the ground-state decay already considered. Experimentally the branch to the 1165-keV 0^+_2 state has $\log f_0 t$ = 6.08(10). The KHH$_e$ (+ PKH) interaction result is $\log f_0 t$ = 5.88 in rather good agreement with experiment. The ^{206}Pb 0^+_2 state is found to have a large $\nu 2p^{-2}_{1/2}$ component — 40% as opposed to 52% in the 0^+_1 state — and this is responsible for the fact that the decay branch is relatively strong even through the level is a classic anticoherent state to the ^{206}Tl ground state.

From data listed in Ref. [51], an experimental beta moment of $B_1^{(2)} = 7.4^{+0.8}_{-2.3}$ fm^2 is derived for the decay branch to the 803-keV 2^+_1 state (the lower limit is due to the possibility of γ feeding from the 0^+_2 state). The KHH$_e$ (+ PKH) prediction of $B_1^{(2)}$ = 3.30 fm^2 is detailed in Table XIII. Two possible reasons for the rather poor agreement are immediately obvious. The first is that the ^{206}Pb 2^+_1 wave function is somewhat in error. To illustrate this possibility, the KHH (+ PKH) prediction is also detailed in Table XIII. For both interactions the first 2^+ state of ^{206}Pb is mainly $\nu 1f^{-1}_{5/2} 2p^{-1}_{1/2}$ and the second 2^+ state is closely orthogonal with a dominant $\nu 2p^{-1}_{3/2} 2p^{-1}_{1/2}$ component. The β^- decay proceeds mainly through the latter configuration since the ^{206}Tl 0^- ground state is almost a pure $\nu 2p^{-1}_{1/2} \pi 2s^{-1}_{1/2}$ state and a $\nu 1f_{5/2} \rightarrow \pi 2s_{1/2}$ transition is Δl forbidden. However, the mixing of the $\nu 1f^{-1}_{5/2} 2p^{-1}_{1/2}$ and $\nu 2p^{-1}_{3/2} 2p^{-1}_{1/2}$ configurations is considerably greater for the KHH interaction than for KHH$_e$ so that, as seen in Table XIII, the unique first-forbidden matrix element is increased. Since $B_1^{(2)} = (M_2^z)^2/4$, the beta moment for the KHH interaction is 5.70 fm^2, in agreement with experiment.

TABLE XIII. The ^{206}Tl(0^-) $\rightarrow$ ^{206}Pb(2_1^+) unique first-forbidden decay calculated with the KHH$_e$ and KHH interactions.

νj_i	πj_f	$D_R(j_ij_f)$		$q_z(j_ij_f)$	$M_2^z(j_ij_f,\text{eff})$	$\mathcal{M}_2^z(j_ij_f)$	
		KHH$_e$	KHH			KHH$_e$	KHH
$0h_{9/2}$	$0g_{7/2}$	+0.0002	+0.0003	0.66[a]	−17.025	− 0.0024	− 0.0031
$1f_{7/2}$	$0g_{7/2}$	+0.0017	+0.0019	0.66[a]	+ 5.056	+ 0.0055	− 0.0232
$1f_{7/2}$	$1d_{5/2}$	+0.0047	+0.0051	0.66[a]	+23.077	+ 0.0714	+ 0.0769
$1f_{7/2}$	$1d_{3/2}$	+0.0211	+0.0233	0.66[a]	+30.199	+ 0.4199	+ 0.4648
$1f_{5/2}$	$0g_{7/2}$	+0.0187	+0.0013	0.66[a]	− 5.206	− 0.0042	− 0.0045
$1f_{5/2}$	$1d_{5/2}$	−0.0212	−0.0242	0.5952	−12.782	+ 0.1610	+ 0.1843
$1f_{5/2}$	$1d_{3/2}$	−0.0181	+0.0214	0.5967	− 9.458	− 0.1023	− 0.1209
$1f_{5/2}$	$2s_{1/2}$	−0.5761	−0.5026		− 0.465[b]	+ 0.2680	+ 0.2338
$2p_{3/2}$	$1d_{5/2}$	+0.0094	+0.0102	0.7316	+14.306	+ 0.0964	+ 0.1062
$2p_{3/2}$	$1d_{3/2}$	+0.0155	+0.0262	0.7118	+ 5.879	+ 0.0651	+ 0.1097
$2p_{3/2}$	$2s_{1/2}$	+0.2312	+0.3273	0.6233	+20.842	+ 3.0031	+ 4.2513
$2p_{1/2}$	$1d_{5/2}$	−0.0542	−0.0460	0.6589	−15.811	+ 0.6471	+ 0.5497
$2p_{1/2}$	$1d_{3/2}$	+0.0423	+0.0633	0.7426	− 3.052	− 0.0956	− 0.1434
$0i_{13/2}$	$0h_{11/2}$	−0.0016	−0.0016	0.66[a]	+32.058	− 0.0341	− 0.0341
$0i_{13/2}$	$0h_{9/2}$	−0.0205	−0.0205	0.3973	+50.809	− 0.4144	− 0.4144
$0i_{11/2}$	$0h_{11/2}$	+0.0306	+0.0306	0.7238	−21.093	− 0.4676	− 0.4676
$0i_{11/2}$	$0h_{9/2}$	+0.0009	+0.0009	0.66[a]	−20.307	− 0.0121	− 0.0121
$1g_{9/2}$	$0h_{11/2}$	+0.0026	+0.0026	0.8420	+11.442	+ 0.0253	+ 0.0253
$1g_{9/2}$	$0h_{9/2}$	+0.0008	+0.0008	0.66[a]	+ 5.673	+ 0.0028	+ 0.0028
$1g_{9/2}$	$1f_{7/2}$	−0.0002	−0.0002	0.66[a]	+25.422	− 0.0039	− 0.0039
$0j_{15/2}$	$0i_{13/2}$	+0.0000	+0.0000	0.66[a]	+34.281	− 0.0007	− 0.0007
		Totals:				+ 3.6308	+ 4.7767

[a] The average value of the ten listed computed values.
[b] From core polarization alone.

The second possible contribution to the small value for the KHH$_e$ beta moment is our neglect of the possible role of an induced operator which breaks the $\Delta l = 2$ selection rule for $R2$ single-particle transitions. The role of such an operator could be important here because the largest $D_R(j_ij_f)$ is that for $\nu 1f_{5/2} \rightarrow \pi 2s_{1/2}$. In contrast, this $D_R(j_ij_f)$ is very small for the ^{205}Hg($\frac{1}{2}^-$) $\rightarrow$ ^{205}Tl($\frac{5}{2}^+$) $R2$ transition discussed in Sec. V A. The Gamow-Teller and unique first-forbidden operators are related since they can be expressed as

$$[\mathbf{r}_{L-1},\boldsymbol{\sigma}]^{\mathrm{L}}\boldsymbol{\tau} \tag{43}$$

with $L = 1$ and 2, respectively. Higher-order corrections to the Gamow-Teller operator are incorporated via the operator [58]

$$p = (8\pi)^{1/2}[r^{L-1}Y^{(L+1)} \otimes \mathbf{s}]^{L}\boldsymbol{\tau} \tag{44}$$

with $L = 1$. A similar operator with $L = 2$ will express the same corrections to unique first-forbidden decays and this operator can connect the $\nu 1f_{5/2}$ and $\pi 2s_{1/2}$ orbits. A theoretical estimate of the matrix element of this operator would be of interest.

F. ^{207}Tl(β^-)^{207}Pb

In addition to the decay rate for ^{207}Tl($\frac{1}{2}^+$) $\rightarrow$ ^{207}Pb($\frac{1}{2_1}^-$) the shape factor for this decay and the decay rate for the $\frac{3}{2_1}^-$ level of ^{207}Pb are known [59, 60]. The decay rate and the shape factor of the ground-state decay were included in the least-squares fit used to determine the effective rank-zero and rank-one operators (Sec. III). The prediction for the ground-state decay rate agrees with experiment to 4.0%. The shape factor is predicted to be

$$C(W) = K(01)[1 + 0.029W - 0.0046/W + 0.0006W^2]. \tag{45}$$

Experimentally, a fit to the first two terms yielded a W term of 0.024 ± 0.008 with no improvement in the fit with a $1/W$ term included [59]. Over the region of W for which the fit was made the predicted $1/W$ and W^2 terms are everywhere less than 8% of the W term. Thus, the predicted and experimental shape factors agree within the experimental uncertainty.

The predicted $\log f_0 t$ value for decay to the $\frac{3}{2_1}^-$ level is 6.20 as compared to the experimental value of 6.24(7). This decay is dominated by $\nu 2p_{3/2} \rightarrow \pi 2s_{1/2}$ for which the contributions of M_1^x are out of phase with those of M_1^u. Hence the decay is weak even though this state is the pygmy resonance for both M_1^u and M_1^x. The predictions for ^{207}Tl decay are seen to give an excellent account of experiment.

G. ^{211}Pb(β^-)^{211}Bi

There is a wealth of information on first-forbidden decays from the β^- decay of ^{211}Pb. The experimental

information [15] is shown on the left in Fig. 6. The lowest-lying even-parity level to which Gamow-Teller decay could occur is predicted with the KHP$_e$ interaction to be the $\frac{7}{2}^+_1$ level at 1821 keV while Q(β^-) = 1379 keV. Thus only $R0$ and $R1$ decays from the $\frac{9}{2}^+$ ^{211}Pb ground state to $\frac{7}{2}^-$, $\frac{9}{2}^-$, and $\frac{11}{2}^-$ of ^{211}Bi are expected to be observed with logf_0t values as small as those shown on the left in Fig. 6. The KHP$_e$ energy spectrum [61] and logf_0t values for the k = 1–5 $\frac{7}{2}^-_k$, $\frac{9}{2}^-_k$, and $\frac{11}{2}^-_k$ levels are shown on the right in Fig. 6. Two sets of theoretical logf_0t values are listed. They differ in the effective $R1$ operators. That labeled (a) is calculated with $sq_x = sq_u$ = 1.00 while (b) uses $sq_x = 1.24$, $sq_u = 0.58$. Both are calculated with $\epsilon_{mec} = 2.0$. The two $R1$ results are given so that the sensitivity of the logf_0t to the possible variation in the sq_x and sq_u allowed by the least-squares fitting to Eq. (32) can be explicitly displayed. Let us consider the individual decays. In this discussion we assume the correspondence between theoretical and experimental levels shown in Fig. 6.

As already discussed the k = 1, 2, 3 $\frac{9}{2}^-_k$ levels are dominated by the $R0$ $\nu 1g_{9/2} \rightarrow \pi 0h_{9/2}$ transition and there is excellent agreement with experiment. All other decays, including those to the k = 4,5 $\frac{9}{2}^-$ levels are dominantly $R1$. The $R2$ contributions are negligible. All fifteen of the calculated $R1$ decays have destructive contributions from M_1^x and M_1^u, i.e., these two matrix elements have the same sign [see Eq. (31)]. Thus, in general, the $R1$ rates are small. From a consideration of the theoretical logf_0t it is expected that the decays to the k = 1–5 $\frac{9}{2}^-$ levels, k = 1–2 $\frac{7}{2}^-$ levels, and k = 3–4 $\frac{11}{2}^-$ levels should be observable. The results for the k = 1–2 $\frac{7}{2}^-$ and k = 3 $\frac{11}{2}^-$ levels are in excellent agreement with our preferred (a) calculation, and the non-observation of the k = 3 $\frac{7}{2}^-$ and k = 1–2 $\frac{11}{2}^-$ decays is consistent with the predictions. Thus excellent overall agreement is achieved for the k = 1–3 decays of all three J^π values. For the remaining four experimental branches there is not enough information to make a meaningful association with theory at this time. Note, for instance, that there are two possibilities for the strong decay to the 1271-keV level: this level could be either $\frac{9}{2}^-_5$ or $\frac{11}{2}^-_4$. The $R1$ rates to the $\frac{9}{2}^-_5$ and $\frac{11}{2}^-_4$ levels are predicted to be relatively strong because M_1^x is unusually large due to coherence of the individual contributions. The $R1$ rates for the k = 3–5 $\frac{7}{2}^-$ levels are unusually weak due to very poor overlap with the ^{211}Pb ground state.

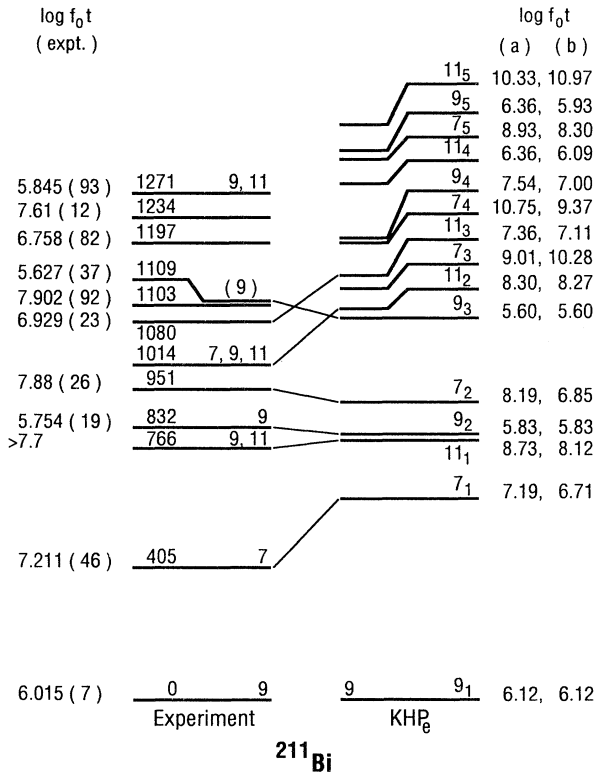

FIG. 6. Comparison to experiment of the KHP$_e$ predictions for the energy spectrum of ^{211}Bi and the ^{211}Pb($\frac{9}{2}^+$) $\rightarrow$ ^{211}Bi logf_0t values. The two predictions for logf_0t use (a) $sq_x = sq_u = 1$, and (b) $sq_x = 1.24$, $sq_u = 0.58$.

VI. DISCUSSION

A. Why the beta moments are so large

The present results provide a somewhat different understanding of the plethora of fast first-forbidden β^- decays in the lead region (*vis-a-vis* lighter nuclei) than was the previous conventional wisdom. The explanations for $R0$ and $R1$ decays differ in some aspects but have the common feature of the "coherency" of the single-particle matrix elements for those transitions which are fast. This "coherency" is quite remarkable — especially for $R0$ decays and leads to the descriptive term pygmy resonance. This coherency is an important contribution to the speed of these decays. It results in large matrix elements even in those cases where the transitions are not very single-particle-like.

For $R1$ decays a well-known important contribution is the increased value of ξ ($\equiv \alpha Z/2r_u$) which is ~3.2 at A = 16 and ~16.3 at A = 208. Since E_γ — given in Eq. (6) — is essentially the Coulomb displacement energy, Eqs. (27)–(28) display the strong dependence of $B_1^{(1)}$ on Z which potentially can enhance it considerably above its value at, say, A = 16 when M_1^u and M_1^x have opposite phases. This dependence on phase is an interesting aspect of $R1$ decays not present for $R0$ decays (since the relative phase of the $R0$ matrix elements is fixed as destructive by fundamental considerations). It causes the dramatic difference in the logf_0t values of the decays to the 1_1^- states of ^{210,212,214}Bi on the one hand and the 1_1^- state of ^{206}Tl and the 1_2^- states of ^{210,212,214}Bi on the other.

In contrast, we find that the $R0$ decays are not enhanced by increasing Z. The ratio M_0^T/M_0^S is roughly

equal to $\hbar\omega$ and as such decreases with increasing A. At the same time a_S is increasing with A. The result is that without mesonic enhancement, i.e., $\epsilon_{\rm mec} = 1$ in Eqs. (27) and (30), the two contributions to $B_0^{(0)}$ would nearly cancel and $B_0^{(0)}$ would be very small indeed. Thus, in our formulation of the problem, there are two reasons for the very large values of the $R0$ beta moment: the large values of M_0^S and M_0^T — due to "coherency" — and the large value of $\epsilon_{\rm mec}$.

B. Comparison of $A \approx 16$ and 208 $\Delta J = 0$ decays

First-forbidden decays in the ^{16}O region have very different characteristics from those in the ^{208}Pb region. First, for ^{16}O, $N = Z$ and the orbits just below the Fermi surface are $0p_{1/2}$ and $0p_{3/2}$ ($Q = 1$) while those just above the Fermi surface are $0d_{5/2}$, $0d_{3/2}$, and $1s_{1/2}$ ($Q = 2$). The two possible $\Delta j = 0$ transitions for, say, ^{16}N$(0^-) \rightarrow {}^{16}O(0^+)$ are $\nu 1s_{1/2} \rightarrow \pi 0p_{1/2}$ and $\nu 0d_{3/2} \rightarrow \pi 0p_{3/2}$. These are both particle-hole transitions so that they add destructively. This leads to the first difference: unlike $\Delta J = 0$ transitions in the ^{208}Pb region, there is no coherency to enhance and stabilize the decay.

The second difference has to do with radial wave functions. The dominant single-particle transition for the faster ΔJ = 0 transitions in the ^{16}O region is $\nu 1s_{1/2} \rightarrow \pi 0p_{1/2}$ [12, 11]. The radial integrals for this transition involve a nodeless orbit and an orbit with one node and thus result from the difference between two large numbers just as for $\nu 1g_{9/2} \rightarrow \pi 0h_{9/2}$. Also $S(n)$ is quite small and the neutron and proton separation energies differ considerably for all the fast decays. The result of these three factors is that the radial integrals are more sensitive to the parameters of the radial wave functions than the $\nu 2p_{1/2} \rightarrow \pi 2s_{1/2}$ transition which dominates the $A = 205$–208 decays [39, 12, 13].

The third difference relates to the effect of np-nh admixtures of which the "final-state" correlations of Fig. 3 are a subset. The fact that $N = Z$ and that $j_p = j_h$ orbitals of opposite parity are available near the Fermi surface means that np-nh admixtures play a more direct and larger role in determining M_0^S and M_0^T at ^{16}O than at ^{208}Pb where $j_h = j_p$ orbitals of opposite parity are not available (see Fig. 2). A serious problem in evaluating the effect of np-nh admixtures at $A \sim 16$ is the slow convergence of the results in an np-nh expansion [13, 62]. The convergence is faster at ^{208}Pb as can be surmised from the large energy denominators in a perturbative treatment. Another way to view the difference is that in the lead region the dominant np-nh admixtures do not contribute directly to the transitions while near ^{16}O they do.

A great deal of effort has gone into determining the effects of np-nh admixtures [3, 11, 10] and inexact knowledge of the radial wave functions [12, 13]. About 10 years ago it was thought that simultaneous consideration of muon capture by ^{16}O and ^{16}N(0^-) β^- decay would give the best value of $\epsilon_{\rm mec}$. It is now clear that this consideration does not resolve the problems in the determination of the $M_0^{S,T}$ discussed above [10]. Rather, the best approach appears to be one similar to that presented here; namely, an omnibus comparison of all relevant $\Delta J = 0$ decays. Such an approach [12, 11] leads to $\epsilon_{\rm mec} \approx 1.64$ in the ^{16}O region.

C. Mesonic enhancement of γ_5

We have made the assumption that $\epsilon_{\rm mec}$ is state independent. Our results would suggest that this assumption is good to within an uncertainty roughly equal to that we term the theoretical uncertainty, ~6%. [Note that an uncertainty in $\epsilon_{\rm mec}$ is equivalent to ~twice that uncertainty in $\overline{C(W)}^{1/2}$.] The justification for this assumption comes from the studies [3, 4, 7, 8] showing that the mec enhancement is expected to be — and actually is — well approximated by a matrix element proportional to that of $\boldsymbol{\sigma}\cdot\mathbf{p}/M$ which is the nonrelativistic form of γ_5.

The only published calculation of the two-body mec contribution for the lead region appears to be that of Kirchbach and Reinhardt [5] who found an enhancement of 40% for the $\nu 2p_{1/2} \rightarrow \pi 2s_{1/2}$ transition in $A = 206$. This result is in serious disagreement with the present findings. Let us discuss the ingredients of this disagreement.

Possible errors in the present calculation. We are looking for a 40–50 % error(s) in our calculations which is systematic enough to be parametrized successfully and leaves the $R1$ decays essentially unaffected. One thinks of np-nh effects such as can be treated by RPA approaches as systematic enough but this is quite unlikely to be the problem for several reasons: (1) Core-polarization contributions are included in the Kuo-Herling effective interaction (we are concerned here with additional effects specific to the operators under consideration), (2) first-order effects on the $R0$ and $R1$ decay are included, (3) the $R1$ predictions are in overall agreement with experiment and higher-order contributions would be expected to have similar effects on the $R0$ and $R1$ decays and to quench the decays rather than the opposite. A more likely possibility has to do with the very large effect of the tensor part of the nucleon-nucleon G matrix on the core-polarization corrections q_S and q_T [40]. Because M_0^S and M_0^T are conjugate operators, we have $1 - q_T \approx -(1 - q_S)$ so that any change in these quenching factors has a magnified effect in the $R0$ beta moment. The large contribution of the tensor part of the interaction is illustrated by the H7B result for the $\nu 2p_{1/2} \rightarrow \pi 2s_{1/2}$ single-particle transition; for it, $q_S = 1 - 0.381 + 0.305$, where the last two terms on the right are the central and tensor contributions, respectively [40]. A 60% reduction in the tensor component, coupled with $\epsilon_{\rm mec} = 1.4$, would give agreement with experiment.

Relativistic effects. Kirchbach and Reinhardt [5] noted that the enhancement of 40% was not enough to bring the $R0$ $\log f_0 t$ values for ^{206}Hg $\rightarrow$ ^{206}Tl $\rightarrow$ ^{206}Pb into agreement with experiment. They proposed the presence of relativistic (or other?) effects which could be parametrized by an effective nucleon mass, M^* via

$$\gamma_5 \xrightarrow{non-rel} \boldsymbol{\sigma}\cdot\frac{\mathbf{p}}{M^*}. \quad (46)$$

The present results would give $M^* \approx 0.7M$ assuming this parametrization to be equally applicable to the one-body and two-body contributions.

VII. CONCLUSION

In conclusion, the result $\epsilon_{\rm mec} = 2.01 \pm 0.05$ is in very poor agreement with the only calculation of the mec effect in the lead region. This calculation would give $\epsilon_{\rm mec} \approx 1.4$ if the enhancement were due to mec effects alone. Either the calculation of Kirchbach and Reinhardt [5] is a severe underestimation of the mec contribution or some other effect is also contributing to the decay. There is no obvious explanation for this discrepancy and so one is lead to consider unobvious explanations. One possibility is that the tensor contribution to the effective nuclear interaction is seriously overestimated. Kirchbach and Reinhardt suggest the possibility of relativistic effects. Certainly, more theoretical work needs to be done to address these questions.

ACKNOWLEDGMENTS

This research was supported by the U. S. Department of Energy under Contract No. DE-AC02-76CH00016. I would like to thank H. Behrens, W. Bühring, and D. H. Wilkinson for interesting and informative discussions on the accuracy of the β decay formalism, N. Poppelier and P. Glaudemans for kindly providing me with details of their SDI interaction and instructions in its use, and G. Herling and J. B. McGrory for communicating input to the KH and KHH$_e$ interactions. D. J. Millener provided valuable counsel. Support from the Alexander-von-Humboldt foundation during the preliminary phases of this study is gratefully acknowledged.

APPENDIX A: SPECTROSCOPIC AMPLITUDES AND EFFECTIVE SEPARATION ENERGIES

In this appendix some details are given of the calculation of spectroscopic factors and $D_R(j)$ for use in evaluating the M_0^S and M_0^T via Eqs. (8)–(15). Since there is experimental data for ^{206}Pb $\rightarrow$ ^{205}Tl+p— but not for the other five $A \rightarrow A-1$ cases considered — we will illustrate our approach in more detail for the ^{206}Tl(0^-) $\rightarrow$ ^{206}Pb(0^+) decay. A secondary motive for presenting these results is the present interest in ^{206}Pb $\rightarrow$ ^{205}Tl+p spectroscopic factors [63]. The calculations were performed with the SDI interaction working in a truncated PKH model space. The truncation consisted of omitting the unique parity $\pi 0i_{13/2}$ and $\nu 0j_{15/2}$ orbits from the PKH model space of Fig. 2.

We first compare the calculations to experiment. SDI spectrum and spectroscopic factors of low-lying ^{205}Tl $\frac{1}{2}^+$, $\frac{3}{2}^+$, and $\frac{5}{2}^+$ states are compared to experiment in Fig. 7 and the relevant energies, $\mathcal{A}(j,i)$ and $\mathcal{S}(j,i)$ values, and D_R are collected in Table XIV. The experimental spectroscopic factors $\mathcal{S}_p$ are from the $(e,e'p)$ analysis of Quint *et al.* [64] for the $\frac{1}{2}^+$ states and the $(\vec{t},\alpha)$ analysis of Flynn *et al.* [65] otherwise. Poppelier and Glaudemans [21] presented E_x and $\mathcal{S}_p$ values for the first ten $\frac{1}{2}^+$ states of ^{205}Tl in their original report of results from the SDI. They did not consider $J > \frac{1}{2}$ states. The good agreement of the present E_x and $\mathcal{S}_p$ values with those of Poppelier and Glaudemans shows that — for $A = 205$ and 206 at least — the $\pi 0i_{13/2}$ and $\nu 0j_{15/2}$ orbits play no significant role in the low-lying states. The comparison to experiment of Fig. 7 indicates satisfactory agreement with experiment. Poppelier and Glaudemans commented on the fact that the total experimental $l_p = 0$ pickup strength is less than predicted and is spread over three states as opposed to being almost entirely confined to the first two in the calculation. From Fig. 7 it is seen that the same situation appears for the $\frac{3}{2}^+$ states, although, in this case, appreciable strength appears in the fourth $\frac{3}{2}^+$ state predicted at 1524 keV (see Table XIV). For $\frac{5}{2}^+$, the bulk of the pickup strength is predicted to lie at ~1550 keV. Experimentally, Flynn *et al.* observed possible $\frac{5}{2}^+$ strength of the same magnitude at 1.8–2.1 MeV. Finally, the $l_p = 5$ pickup strength to $\frac{11}{2}^-$ states is predicted to reside mostly in the first, second, third, and sixth states with $E_x : \mathcal{S}_p$ values of 1743:7.30, 2510:2.46, 2580:0.55, 2978:0.55. Again, Flynn *et al.* observed possible $l_p = 5$ strength of comparable magnitude in the 1.5–2.6 MeV region.

The dimensions $D(J)$ of the J matrices for the three cases of Table XIV are $D(\frac{1}{2}^+) = 2072$, $D(\frac{3}{2}^+) = 3983$, and $D(\frac{5}{2}^+) = 5606$. In spite of these rather large dimensions it is seen that the first 20 states or less contain the bulk of the spectroscopic strength. In evaluating the $\langle E_{xj}\rangle$ for use with Eq. (14) the remaining contribution to the $D_R(j)$ not contained in the first 20 states, i.e., $\sum_{i=21,D(J)} D_R(j,i)$, was assumed to lie in the 20th state. The evaluation of the $M_0^{S,T}$ via Eq. (14) is summarized in Table III for the three $\Delta J = 0$ decays considered in this appendix.

APPENDIX B: CONTRIBUTION OF HIGHER-ORDER TERMS TO THE RANK-ZERO BETA DECAY RATE

In this discussion of higher-order terms we confine ourselves to the rank-zero contribution to the β-decay rate. For first-forbidden decays, the shape factor $C(W)$ is an incoherent sum of rank 0, 1, and 2 shape factors, i.e.,

$$C(W) = \sum_R C^{(R)}(W) = \sum_{\mathcal{N},R} K(\mathcal{N}R) W^{\mathcal{N}}. \quad (B1)$$

In normal order, we use the expressions for the $K(\mathcal{N}R)$ given by Warburton *et al.* [13]. In the Behrens-Bühring treatment the rank-zero shape factor is given by (Eq. (7.56) of Ref. [19])

$$C^{(0)}(W) = M_0^2(1,1)+m_0^2(1,1)-\frac{2\mu_1\gamma_1}{W}M_0(1,1)m_0(1,1), \quad \text{(B2)}$$

where R specifies the rank of the operators and W is the electron energy. In Eq. (B2), the $M_0(1,1)$ and $m_0(1,1)$ are defined as simultaneous expansions in powers of the three parameters αZ, $m_e r_u$, and $W r_u$ times form factor coefficients F^N_{KLs} and $F^N_{KLs}(1,m,n,\rho)$. The form factor coefficients F^0_{KLs} are simply related to nuclear matrix elements. Thus, the M_0^S and $\epsilon_{\rm mec}M_0^T$ — of paramount importance in rank-zero decay — are defined by $M_0^S = -r_u F^0_{011}$ and $\epsilon_{\rm mec}M_0^T = F^0_{000}$. The $F^N_{KLs}(1,m,n,\rho)$ are obtained from the F^N_{KLs} by including in the radial integral an extra factor $I(1,m,n,\rho)$, e.g., Eq. (17). The $I(1,m,n,\rho)$ only occur in terms containing powers of αZ; explicitly, $I(1,m,n,\rho)$ accompanies $(\alpha Z)^\rho$ and $I(1,m,n,0) \equiv 1$. Algebraic expressions for the $I(1,m,n,\rho)$ are given by Behrens and Bühring (Table 4.3 of Ref. [19]). The $F^N_{KLs}(1,m,n,\rho)$ (including $\rho = 0$) are obtained from the $F^0_{KLs}(1,m,n,\rho)$ by including in the radial integral an extra factor $(r/r_u)^{2N}$. Because we are interested in the relative size of the higher-order terms, it is convenient to introduce the ratios

TABLE XIV. SDI results connecting the low-lying $\frac{1}{2}^+$, $\frac{3}{2}^+$, and $\frac{5}{2}^+$ levels of ^{205}Tl to the 0^-, and 0^+ ground states of ^{206}Tl and ^{206}Pb. The neutron and proton separation energies $S(n)$ and $S(p)$ of ^{206}Tl and ^{206}Pb, respectively, are based on experiment when known while E_x is the model energy. All three of these energies are in keV. D_0(j,i) is for ^{206}Tl → ^{206}Pb.

i	E_x	$\mathcal{A}_n$	$\mathcal{A}_p$	$D_0(j;i)$	$\mathcal{S}_n$	$\mathcal{S}_p$	$S(n)$	$S(p)$
				$j^\pi = \frac{1}{2}^+$				
1	0	0.726	−1.121	−0.575	0.527	1.256	6504	7252
2	1282	0.256	−0.718	−0.130	0.065	0.516	7722	8470
3	1447	−0.541	0.063	−0.024	0.293	0.004	7938	8686
4	1586	0.130	−0.106	−0.010	0.017	0.011	8090	8838
5	1612	0.401	0.184	0.052	0.160	0.034	8116	8864
$\sum_{i=1,20}$ =				−0.698	1.156	1.887		
$D_0(j)$, $\overline{n}(j)$, $\overline{p}(j)$ =				−0.696	1.221	1.999		
				$j^\pi = \frac{3}{2}^+$				
1	124	0.448	1.536	0.344	0.201	2.360	6708	7456
2	1222	0.325	−1.065	−0.173	0.105	1.135	7645	8393
3	1442	−0.065	0.104	−0.003	0.004	0.011	7845	8593
4	1524	−0.637	0.451	−0.144	0.406	0.204	8108	8856
5	1576	−0.244	−0.133	0.016	0.059	0.018	8160	8908
$\sum_{i=1,20}$ =				0.054	3.590	3.778		
$D_0(j)$, $\overline{n}(j)$, $\overline{p}(j)$ =				0.074	3.835	3.998		
				$j^\pi = \frac{5}{2}^+$				
1	753	−1.130	0.672	−0.310	1.277	0.451	7323	8071
2	1428	1.122	−0.055	−0.025	1.259	0.003	7684	8432
3	1604	−1.124	−0.109	0.050	1.264	0.012	7974	8722
4	1681	1.232	0.012	0.006	1.518	0.000	8051	8799
5	1744	−0.158	−0.144	0.009	0.025	0.021	8114	8862
6	1892	0.196	−0.107	−0.009	0.039	0.011	8262	9010
7	1958	0.219	0.032	0.003	0.048	0.001	8328	9076
8	2139	0.231	0.255	0.024	0.053	0.065	8509	9257
9	2188	−0.201	− 0.356	0.029	0.041	0.127	8558	9306
10	2292	0.270	1.585	0.175	0.073	2.513	8662	9410
11	2320	0.188	1.131	0.086	0.035	1.279	8690	9438
12	2358	−0.277	0.618	−0.070	0.077	0.382	8728	9476
$\sum_{i=1,20}$ =				−0.046	5.751	5.262		
$D_0(j)$, $\overline{n}(j)$, $\overline{p}(j)$ =				−0.060	5.934	5.989		

$$r_S^N(1,m,n,\rho) = F_{011}^N(1,m,n,\rho)/F_{011}^0,$$
$$r_T^N(1,m,n,\rho) = F_{000}^N(1,m,n,\rho)/F_{000}^0. \quad \text{(B3)}$$

Thus r'_w of Sec. III D 1 is equivalent to $\frac{2}{3}r_S^0(1,1,1,1)$.

With these definitions we can now incorporate the second and third order terms which might influence the β decay rate. In this we follow Wiesner *et al.* [45] who made a detailed and careful study of the effects of higher-order terms on $^{206}\mathrm{Hg}(0^+) \rightarrow {}^{206}\mathrm{Tl}(0^-)$. For the $K(\mathcal{N}0)$ of Eq. (B1) we find

$$K(00) = \zeta_0^2 + \tfrac{1}{9}(M_0^S)^2,$$
$$K(10) = -\tfrac{2}{9}\alpha Z r_u r_T^1(1,1,1,1)\epsilon_{\mathrm{mec}} M_0^T, \quad \text{(B4)}$$
$$K(-10) = -\tfrac{2}{3}\mu_1\gamma_1\zeta_0 M_0^S[1 - \tfrac{1}{10}(\alpha Z)^2 r_S^1(1,3,2,2)]$$

with

$$\zeta_0 \equiv M_1^{(0)} = q_2\epsilon_{\mathrm{mec}} M_0^T + a_S M_0^S,$$
$$q_2 = 1 - \tfrac{1}{6}(\alpha Z)^2 r_T^1(1,2,2,2), \quad \text{(B5)}$$

$$a_S = [r'_w - \tfrac{1}{15}(\alpha Z)^2 r_S^1(1,3,3,3)]\xi + \tfrac{1}{3}W_0$$
$$= \tfrac{2}{3}[r_S^0(1,1,1,1) - \tfrac{1}{10}(\alpha Z)^2 r_S^1(1,3,3,3)]\xi + \tfrac{1}{3}W_0. \quad \text{(B6)}$$

In evaluating the relative importance of the higher-order terms in the lead region we use $\alpha Z = 0.6$, $r_u = 0.0184$, and $W_0 \leq 4.57$ (see Table I). Values for the $r_{S,T}^N(1,m,n,\rho)$ calculated by numerical differentiation and integration with HO wave functions ($b = 2.490$ fm) are listed in Table XV for the orbits of interest. A check on the numerical calculations is provided by the fact that analytic expressions for M_0^S, M_0^T, and r_T^1 are available for HO wave functions. For r_T^1 an expression given by Rose and Osborne [66] can be used to give

$$r_T^1 = \frac{1}{3}\left[\frac{\mathcal{F}_3}{b^2\mathcal{F}_1} - (2l+3)\right]\left(\frac{b}{r_u}\right)^2, \quad \text{(B7)}$$

where

$$\mathcal{F}_L = \int_0^\infty r^{L+2}\mathcal{R}_{nl}\mathcal{R}_{n'l'}\,dr, \quad \text{(B8)}$$

the $\mathcal{R}_{nl}$ are HO wave functions, $l = l' + 1$, and $n = n'$ or $n' - 1$. Thus the r_T^1 of Table XV are simple multiples of $\frac{1}{2}(b/r_u)^2 = 0.1233/2$.

There is also a second-order W^2 term, $K(20) = -\frac{1}{18}r_u^2 r_T^1 \epsilon_{\mathrm{mec}} M_0^T$, which we do not include since it is of negligible importance to the decay rate, i.e.,

$$K(20)W^2/K(10)W \leq \frac{r_u W_0}{4\alpha Z} \leq 0.035. \quad \text{(B9)}$$

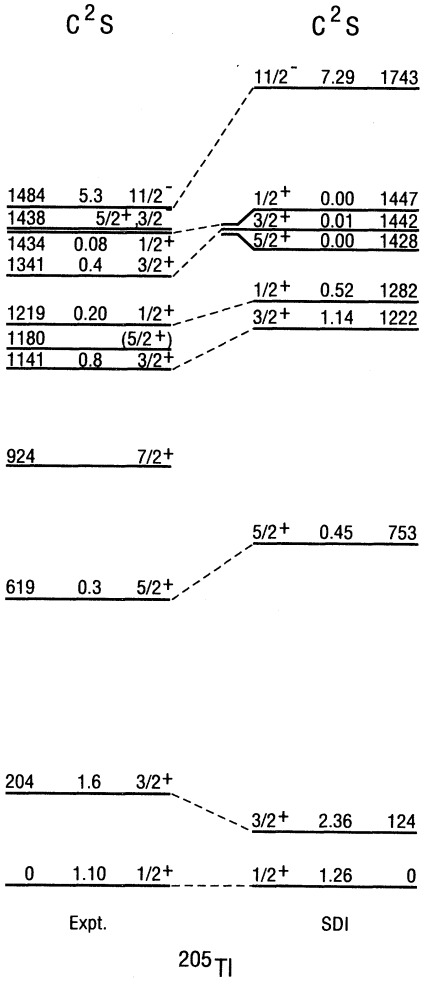

FIG. 7. Comparison to experiment of the Poppelier-Glaudemans SDI predictions for the energy spectrum of $^{205}\mathrm{Tl}$ and for $^{206}\mathrm{Pb} \rightarrow {}^{205}\mathrm{Tl}$ + p spectroscopic factors (C^2S).

TABLE XV. Ratios of radial integrals calculated with harmonic oscillator wave functions with an oscillator length b = 2.490 fm. The listed integrals are for the five possible $\Delta j = 0$ particle-hole → vacuum transitions involving the orbits of Fig. 2. The values of $M_0^S(j)$ and $M_0^T(j)$ (in fm) are also listed.

	orbits				
Quantity	$\frac{1}{2}$	$\frac{3}{2}$	$\frac{5}{2}$	$\frac{9}{2}$	$\frac{11}{2}$
$M_0^S(j_i j_f)$	8.304	8.877	16.309	9.925	27.720
$M_0^T(j_i j_f)$	108.8	116.3	213.6	130.0	363.1
$r_S^0(1,1,1,1)$	1.1902	1.1489	1.2256	1.0281	1.2248
r_T^1	0.3081	0.1233	0.4316	0.0000	0.6782
$r_T^1(1,1,1,1)$	0.4282	0.2513	0.5696	0.2102	0.8631
$r_T^1(1,2,2,1)$	0.4436	0.2398	0.5967	0.1640	0.9130
$r_T^1(1,2,2,2)$	0.6244	0.3864	0.8237	0.3570	1.2388
$r_S^1(1,3,2,2)$	1.7642	2.0640	1.5940	2.5901	1.6251
$r_S^1(1,3,3,3)$	2.0220	2.3488	1.8733	2.8257	1.9484

We have dropped a similar term, $-\frac{1}{9}W_0 r_u^2 r_T^1 \epsilon_{\rm mec} M_0^T$ [$\equiv 2K(20)W_0$] from both $K(10)$ and $K(-10)$ because in both cases it is also of negligible importance to the decay rate. A simplification has been made in $K(10)$: we have made the approximation $I(1,2,2,1) = I(1,1,1,1)$ which is true enough so that it will generate negligible error. All of $K(20)$ is from second order and the $(\alpha Z)^2$ term in $K(-10)$ is from third order. The rest of the higher-order terms are contained in ζ_0 which differs from our first-order definition (Sec. II) in the introduction of q_2 and a modification to a_S. For the latter a third-order term in $(\alpha Z)^2$ has been subtracted from $r_S^0(1,1,1,1)$. The factor q_2 modifies $\epsilon_{\rm mec} M_0^T$ by another $(\alpha Z)^2$ term. Once again we have neglected terms in $W_0 r_u$ and r_u because of their relative unimportance, in this case, $-\frac{1}{9}(\alpha Z W_0 r_u - \frac{3}{2} r_u^2) r_T^1$ has been dropped from q_2.

We illustrate the relative importance of the lesser first-order terms and the higher-order terms by a calculation for the ^{206}Hg$(0^+) \rightarrow {}^{206}Tl(0^-)$, single-particle $\pi 2s_{1/2}^{-2} \rightarrow \nu 2p_{1/2}^{-1} \pi 2s_{1/2}^{-1}$ transition carried out with the HO parameters of Table XV. In this calculation we use $q_S = q_T = 1.0$ and $\epsilon_{\rm mec} = 1.61$. This value of $\epsilon_{\rm mec}$ gives agreement with the experimental beta moment $B_1^{(0)} = 59 \pm 6$ fm^2 when used with the single-particle $M_0^{S,T}$ of Table XV. The results, listed in Table XVI, are entirely representative of more realistic calculations and of other transitions. It is seen that the higher-order effects are indeed quite small and can be neglected.

The W term, $K(10)$, was retained in Eq. (B4) in spite of its small effect on the decay rate because of its potential importance in the determination of $\epsilon_{\rm mec}$. Unlike the decay rate, $K(10)$ is dependent on $\epsilon_{\rm mec} M_0^T$ alone (i.e., not in combination with M_0^S) and thus its measurement would offer an attractive alternative method of assessing the mesonic effect on M_0^T. Wiesner et al. [45] did indeed make a careful measurement of the ^{206}Hg$(0^+) \rightarrow {}^{206}Tl(0^-)$ shape factor from which they extracted, via a least-squares fit, values for $K(00)$, $K(-10)$, and $K(10)$. Tantalizingly enough, the result for $K(10)$ was twice as large as predicted from the impulse approximation, and thus consistent with $\epsilon_{\rm mec} \sim 2.0$. However, no uncertainties were given and they were probably rather large. A measurement of the shape factor accurate enough to give $K(10)$ with an uncertainty of $\sim$10% would be of great value.

TABLE XVI. Relative contributions of various terms to the ^{206}Hg$(0^+) \rightarrow {}^{206}Tl(0^-)$ single-particle $\pi 2s_{1/2}^{-2} \rightarrow \nu 2p_{1/2}^{-1} \pi 2s_{1/2}^{-1}$ decay calculated with harmonic oscillator wave functions with an oscillator length $b = 2.490$ fm, $q_{S,T}(\frac{1}{2}) = 1.0$, and $\epsilon_{nn} = 1.61$.

Term	Order	% contribution or value
$\frac{1}{9}(M_0^S)^2$	1st	+0.22%
$K(-10)$	1st	+4.1%
$K(10)$	2nd	−0.010%
q_2	2nd	0.964
$\frac{a_S(\text{1st} + \text{2nd order})}{a_S(\text{1st order})}$	2nd	0.946
2nd order change in $f_0 t$	2nd	−1.09%

APPENDIX C: HIGHER-ORDER RADIATIVE CORRECTIONS AND NUCLEAR SIZE EFFECTS

1. Radiative corrections

The Wilkinson-Macefield [47] parametrization of the allowed β decay phase space factor f_0 contains the "outer" radiative correction to order α [67]. This is adequate for $Z < 30$ but for $Z \sim 82$ higher-order terms will contribute measurably to the decay rate and other observables and it is not presently clear as to how to make these corrections. A rough guess as to their magnitude can be made based on the studies aimed to determine them accurately for superallowed Fermi transitions [68–70]. These higher-order terms are of order $Z\alpha^2$, $Z^2\alpha^3$, $Z^3\alpha^4$, etc. The first two of these are discussed explicitly by Jaus and Rasche [68] and by Sirlin [69] and at $Z = 82$ together increase the decay rate by $\sim$4%. We might expect terms of order $Z^3\alpha^4$ and higher to contribute an additional increase of $O(Z^3\alpha^4 \ln(M)/(1-\alpha Z)) \approx 3\%$. So the total effect of higher-order "outer" radiative corrections *might* increase the decay rate of hypothetical superallowed Fermi decays in the lead region by $\sim$7%. The question of how this relates to axial currents is presently not understood. However, it probably represents a good guess as to the magnitude of the effect. A 7% increase in the $R0$ decay rate would result in a decrease in $\epsilon_{\rm mec}$ of $\sim$1.8%.

2. Size effects

One of the corrections to the basic Fermi function $F(Z,W)$—calculated for a point nucleus—is the convolution of the lepton and nucleon wave functions over the nuclear volume. Wilkinson [71] has recently presented a more accurate (for $Z < 60$) calculation of this correction $C(Z,W)$ based on the Behrens-Bühring formalism [19]. $C(Z,W)$ deviates $\sim$14% from unity near ^{208}Pb for low $Q(\beta^-)$ values. These new results give a $C(Z,W)$ at low $Q(\beta^-)$ and $Z = 82$ such that f_0 is larger by 2.9% than the Wilkinson-Macefield treatment [70]. There are several sources of uncertainty in both the old and new calculations of $C(Z,W)$: (1) In the new version the accuracy of the calculation is not verified for $Z > 60$; (2) in the expansion of $C(Z,W)$ in terms of the nuclear parameters (see Sec. III D 1), terms higher than $n = 1$ in $(\alpha Z)^{2n}$ were not considered and $(\alpha Z)^4 \approx 0.13$; and (3) the convolution uses single-nucleon wave functions which are uniform throughout the nucleus rather than realistic radial wave functions. It is conceivable that these three effects could cause an uncertainty $O((\alpha Z)^4 \approx 13\%)$ in $1 - C(Z,W)$ so that correcting f_0 for these deficiencies could cause f_0 to be $\sim$5% larger than calculated here with the result that $\epsilon_{\rm mec}$ would be $\sim$1.3% smaller.

3. Summary

The two effects discussed in this appendix could conceivably increase the calculated value of f_0 by ~12%. This is a large enough correction to be of concern in nuclear structure studies such as the present one. It would appear desirable to attempt more refined calculations of these and other possible effects on f_0 at $Z \sim 82$.

APPENDIX D: THE EXPERIMENTAL BETA MOMENT FOR ^{205}Pb($\frac{5}{2}^-$) $\rightarrow$ ^{205}Tl($\frac{1}{2}^+$) EC DECAY

The decay of ^{205}Pb by electron capture is unusual in that the available disintegration energy, Q(EC) = 51.3 ± 0.6 keV [53] is very small — not even large enough to allow capture from the K shell. Furthermore, the transition is first-forbidden unique. For these two reasons it is dominated by capture from the $p_{3/2}$ atomic shells, i.e., LIII, MIII, NIII, and OIII [72]. We are interested in the $f_1^U t$ value and thus in the evaluation of f_1^U and the half-life t. The unique first-forbidden f_1^U value of interest is given by [72]

$$f_1^U = \frac{\pi}{2}[P_L + P_M + P_N + P_O], \tag{D1}$$

where the P_x ($x = L, M, N, O$) are the probability of capture from the indicated atomic orbit. The P_x are given by

$$P_x = q_{x1}^4 \beta_{x1}^2 + q_{x2}^4 \beta_{x2}^2 + q_{x3}^2 p_{x3}^2 \beta_{x3}^2 + q_{x4}^2 p_{x4}^2 \beta_{x4}^2, \tag{D2}$$

where the xn refer to LI, LII... MI, etc., and p and q are the electron and neutrino momenta with

$$q_{xn} = Q(\text{EC}) - E_{xn} - E_R. \tag{D3}$$

In Eq. (D3), E_{xn} is the binding energy of the captured electron in the daughter atom and E_R is the rearrangement energy for which we use the approximate relationship of Bahcall [52] which yields 133 eV. Using the β_{xn} and $\beta_{xn}p_{xn}$ of Mann and Waber [73] listed by Bambynek *et al.* [72], we find

$$f_1^U = \frac{\pi}{2}(4.428 + 2.006 + 0.567 + 0.102) \times 10^{-4} = 1.116 \times 10^{-3} \tag{D4}$$

with an uncertainty of 3% due to that in Q(EC).

The evaluation of f_1^U is given in some detail to clearly expose its dependence on Q(EC). This is felt desirable because there has been conflicting evidence as to the best experimental value of Q(EC). Pengra, Genz, and Fink [74] measured the M/L and N/M electron capture ratios and obtained values of 0.525(8) and 0.271(10), respectively. Using Eqs. (D2)–(D3) and working backward from these ratios, a value Q(EC) = 41.4 ± 1.1 keV is obtained as opposed to the latest mass-evaluation [75] result of 53.5 ± 1.6 keV and the recent measurement [53] of 51.3 ± 0.6 keV. For Q(EC) = 41.4 keV, we find $f_1^U = 0.633 \times 10^{-3}$. However, it should be stressed that the measured value [74] of the N/M ratio is 2.4 standard deviations from the value expected for Q(EC) = 41.4 keV, i.e., the two ratios are not consistent. Thus, there is reason to doubt the experimental results or the ancillary measurements or theory used to interpret them. We use the recent result for Q(EC) of 51.3 ± 0.6 keV, but the discrepency should be kept in mind.

The half-life also depends on Q(EC). This dependence arises because it is evaluated from the L x-ray activity as measured by Wing, Stephens, and Huizenga [76]. These authors results can be expressed as

$$t = (3.0 \pm 0.32)\left(\frac{\overline{\omega}_L}{0.40} \times \frac{P_L}{\sum_x P_x}\right) \times 10^7 \text{ y}. \tag{D5}$$

Using $\overline{\omega}_L = 0.333$ [74] and the P_x of Eq. (D2), we find $t = (1.56 \pm 0.17) \times 10^7$ y, $f_1^U t = (5.48 \pm 0.60) \times 10^{11}$, and $\log f_1^U t = 11.74 \pm 0.04$ for Q(EC) = 51.3 ± 0.6 keV.

The beta moment $B_1^{(2)}$ is given by [13, 77] $10^{-6} B_1^{(2)} = 2758/f_1^U t$ fm^2. For Q(EC) = 51.3 keV we have $B_1^{(2)} = (5.0 \pm 0.6) \times 10^{-3}$ fm^2.

[1] K. Kubodera, J. Delorme, and M. Rho, Phys. Rev. Lett. **40**, 755 (1978).

[2] P. Guichon, M. Giffon, J. Joesph, R. Laverrière, and C. Samour, Z. Phys. A **285**, 183 (1978); P. Guichon, M. Giffon, and C. Samour, Phys. Letts. **74B**, 15 (1978).

[3] I. S. Towner and F. C. Khanna, Nucl. Phys. **A372**, 331 (1981).

[4] J. Delorme, Nucl. Phys. **A374**, 541c (1982).

[5] M. Kirchbach and M. Reinhardt, Phys. Lett. **208**, 79 (1988). The result $\epsilon_{\text{mec}} = 0.45$ for $A = 96$ given in the reference has been revised to $\epsilon_{\text{mec}} = 0.60$ (M. Kirchbach, private communication).

[6] M. Kirchbach, in *Proceedings of the International Symposium on Modern Developments in Nuclear Physics, Novosibirsk, U.S.S.R.*, edited by O. P. Sushkov (World-Scientific, Singapore, 1987), p. 475.

[7] E. G. Adelberger, M. M. Hindi, C. D. Hoyle, H. E. Swanson, R. D. Von Lintig, and W. C. Haxton, Phys. Rev. C **27**, 2833 (1983).

[8] I. S. Towner, Comments Nucl. Part. Phys. **15**, 145 (1986).

[9] I. S. Towner, Phys. Rep. **155**, 263 (1987).

[10] W. C. Haxton and C. Johnson, Phys. Rev. Lett. **65**, 1325 (1990).

[11] E. K. Warburton, in *Interactions and Structures in Nuclei*, edited by R. J. Blin-Stoyle and W. D. Hamilton (Hilger, Bristol/Philadelphia, 1988), p. 81.

[12] D. J. Millener and E. K. Warburton, in *Nuclear Shell Models*, edited by M. Vallieres and B. H. Wildenthal (World-Scientific, Singapore, 1985), p. 365.

[13] E. K. Warburton, J. A. Becker, B. A. Brown, and D. J. Millener, Ann. Phys. (N.Y.) **187**, 471 (1988).

[14] H. Mach, E. K. Warburton, R. L. Gill, R. F. Casten, J. A. Becker, B. A. Brown, and J. A. Winger, Phys. Rev. C **41**, 226 (1990).
[15] National Nuclear Data Center on-line retrieval system.
[16] J. Damgaard, R. Broglia, and C. Riedel, Nucl. Phys. **A135**, 310 (1969).
[17] H. Ejiri and J. I. Fujita, Phys. Rep. **38C**, 85 (1978).
[18] F. Krmpotic, K. Ebert, and W. Wild, Nucl. Phys. **A342**, 497 (1980).
[19] H. Behrens and W. Bühring, *Electron Radial Wave Functions and Nuclear Beta-Decay* (Clarendon, Oxford, 1982).
[20] B. A. Brown, A. Etchegoyen, W. D. M. Rae, and N. S. Godwin, OXBASH, 1984 (unpublished).
[21] N. A. F. M. Poppelier and P. W. M. Glaudemans, Z. Phys. A **329**, 275 (1988).
[22] T. T. S. Kuo and G. H. Herling, U.S. Naval Research Laboratory Report No. 2258, 1971 (unpublished).
[23] T. T. S. Kuo and G. E. Brown, Nucl. Phys. **85**, 40 (1966).
[24] T. Hamada and I. D. Johnston, Nucl. Phys. **34**, 382 (1962).
[25] J. B. McGrory and T. T. S. Kuo, Nucl. Phys. **A247**, 283 (1975).
[26] E. K. Warburton and B. A. Brown, Phys. Rev. C **43**, 602 (1991).
[27] I. Bergstrom, J. Blomqvist, C. J. Herrlander, and C. G. Lindeén, Research Institute of Physics (Stockholm, Sweden) Annual Report, 3.3.14 (1976).
[28] L. Rydstrom, J. Blomqvist, R. J. Liotta, and C. Pomar, Nucl. Phys. **A512**, 217 (1990).
[29] J. B. McGrory, private communication.
[30] A. Hosaka, K.-I. Kubo, and H. Toki, Nucl. Phys. **A244**, 76 (1985).
[31] The Coulomb contribution to the pp TBME averages 230 keV for the diagonal elements with a spread of $\pm \approx 50$ keV. The off-diagonal TBME are in the range $\pm$ 30 keV.
[32] M. Lacombe, B. Loiseau, J. M. Richard, R. Vinh Mau, J. Côté, P. Pirès, and R. de Tourreil, Phys. Rev. C **21**, 861 (1980).
[33] T. T. S. Kuo, Nucl. Phys. **A122**, 325 (1968).
[34] K. H. Maier, private communication (1989).
[35] M. J. Martin, Nucl. Data Sheets **47**, 797 (1986).
[36] M. S. Antony, J. Britz, and A. Pape, At. Data Nucl. Data Tables **40**, 9 (1988).
[37] H. F. Schopper, *Weak Interactions and Nuclear Beta Decay* (North-Holland, Amsterdam, 1966).
[38] J. Streets, B. A. Brown, and P. E. Hodgson, J. Phys. G. **8**, 839 (1982).
[39] D. J. Millener, D. E. Alburger, E. K. Warburton, and D. H. Wilkinson, Phys. Rev. C **26**, 1167 (1982); E. K. Warburton, D. E. Alburger, and D. J. Millener, *ibid.* **29**, 2281 (1984).
[40] E. K. Warburton, Phys. Rev. C **42**, 2479 (1990).
[41] H. Behrens and W. Bühring, Nucl. Phys. **A162**, 111 (1971).
[42] B. A Brown, C. R. Bronk, and P. E. Hodgson, J. Phys. G **10**, 1683 (1984).
[43] The effect of higher-order terms on the $R1$ beta moment have been considered by Behrens and collaborators, e.g., Ref. [44]. For $\log f_0 t$ values $> \sim 7$ it is not safe to neglect them.
[44] H. Behrens and L. Szybisz, Nucl. Phys. **A223**, 268 (1974).
[45] W. Wiesner, D. Flothmann, H. G. Gils, R. Löhken, and H. Rebel, Nucl. Phys. **A191**, 166 (1972).
[46] Wiesner *et al.* (Ref. [45]) considered ^{206}Tl $\rightarrow$ ^{206}Pb in a shell-model space including $j = \frac{1}{2}, \frac{3}{2}, \frac{5}{2}$, and $\frac{13}{2}$ orbits. The wave functions for these terms were remarkedly similar to the present SDI results [see, e.g., the $D_0(j)$ of Table XIV]. Their calculation differs from the present ones in the omission of the important $j = \frac{11}{2}$ orbits, core-polarization corrections, use of pre-1969 Woods-Saxon wave functions, and — since the work was done before 1978 — neglect of the mec. Nevertheless, their results — viewed in retrospect — clearly indicate the need for a large mec effect.
[47] D. H. Wilkinson and B. E. F. Macefield, Nucl. Phys. **A232**, 1 (1974).
[48] N. B. Gove and M J. Martin, Nucl. Data Tables **10**, 206 (1971); program LOGFT: National Nuclear Data Center on-line retrevial system.
[49] I. S. Towner, Nucl. Phys. **A151**, 97 (1970).
[50] Z. Berant, R. B. Shuhmann, D. E. Alburger, W. T. Chou, R. L. Gill, E. K. Warburton, and C. Wesselbourg, Phys. Rev. C **43**, 1639 (1991).
[51] M. P. Webb, Nucl. Data Sheets **26**, 145 (1979).
[52] J. N. Bahcall, Rev. Mod. Phys. **50**, 881 (1978).
[53] H. Lindner, H. Trieb, T. von Egidy, H. Hiller, J. Klora, U. Mayerhofer, A. Walter, and A. H. Wapstra, Nucl. Instrum. Methods **A297**, 217 (1990).
[54] J. Weneser and G. Friedlander, Science **235**, 755 (1987); G. Friedlander and J. Weneser, *ibid.* **235**, 760 (1987).
[55] E. Braun and I. Talmi, in *Proceedings of the Heidelberg Symposium on Weak and Electromagnetic Interactions in Nuclei*, edited by H.V. Klapdor (Springer, Berlin, 1986).
[56] K. Ogawa and K. Arita, Nucl. Instrum. Methods **A271**, 280 (1988).
[57] As discussed in Sec. III D, the calculations of neutrino-capture parameters described here use $\mu_1 = \lambda_2 = 1$. This is adequate near threshold but at sufficiently high values of W_e accurate values for these parameters should be used since they occur in energy-dependent terms.
[58] B. A. Brown and B. H. Wildenthal, Phys. Rev. C **28**, 2397 (1983).
[59] J. M. Trischuk and E. Kankeleit, Nucl. Phys. **A90**, 33 (1967).
[60] M. R. Schmorak, Nucl. Data Sheets **43**, 383 (1984).
[61] The complete KHP$_e$ spectrum of ^{210,211,212}Bi or details on their wave functions are available upon request to the author.
[62] E. K. Warburton, J. A. Becker, and B. A. Brown, Phys. Rev. C **41**, 1147 (1990).
[63] P. Woldt, P. Grabmayr, G. Rau, G. J. Wagner, M. A. Hofstee, J. M. Schippers, S. Y. Van Der Werf, and H. Nann, Nucl. Phys. **A518**, 496 (1990).
[64] E. N. M. Quint *et al.*, Phys. Rev. Lett. **58**, 1088 (1987).
[65] E. R. Flynn, R. A. Hardekopp, J. D. Sherman, J. W. Sunier, and J. P. Coffin, Nucl. Phys. **A279**, 394 (1977).
[66] M. E. Rose and R. K. Osborne, Phys. Rev. **93**, 1326 (1954).
[67] D. H. Wilkinson, in *Ecole d'Eté de Physique Théorique, Session XXX*, edited by R. Balian, M. Rho, and G. Ripka (Amsterdam, North-Holland, 1977), pp. 879–1017.
[68] W. Jaus and G. Rasche, Phys. Rev. D **35**, 3420 (1987).
[69] A. Sirlin, Phys. Rev. D **35**, 3423 (1987).
[70] D. H. Wilkinson, private communication.

[71] D. H. Wilkinson, Nucl. Instrum Methods **A290**, 509 (1990).
[72] W. Bambynek, H. Behrens, M. H. Chen, B. Crasemann, M. L. Fitzpatrick, K. W. D. Ledingham, H. Genz, M. Mutterer, and R. L. Intemann, Rev. Mod. Phys. **49**, 77 (1977); *ibid.* **49**, 161 (1977).
[73] J. B. Mann and J. T. Waber, Atomic Data **5**, 201 (1973); and private communication to Bambynek *et al.*
[74] J. G. Pengra, H. Genz, and R. W. Fink, Nucl. Phys. **A302**, 1 (1978).
[75] A. H. Wapstra and G. Audi, Nucl. Phys. **A432**, 1 (1985).
[76] J. Wing, C. M. Stevens, and J. R. Huizenga, Phys. Rev. **111**, 590 (1958).
[77] D. E. Alburger and E. K. Warburton, Phys. Rev. C **38**, 1843 (1988).